The Plant Cell, Vol. 27: 1477–1496, May 2015, www.plantcell.org

Structures, Functions, and Interactions of ClpT1 and ClpT2 in the Clp Protease System of Arabidopsis Chloroplasts

Jitae Kim,[a] Matthew S. Kimber,[b] Kenji Nishimura,[a] Giulia Friso,[a] Lance Schultz,[b] Lalit Ponnala,[c] and Klaas J. van Wijk[a,1]

[a] Department of Plant Biology, Cornell University, Ithaca, New York 14853
[b] Department of Molecular and Cellular Biology, University of Guelph, Guelph, Ontario N1G 2W1, Canada
[c] Computational Biology Service Unit, Cornell University, Ithaca, New York 14853

ORCID ID: 0000-0001-9536-0487 (K.J.v.W.)

Plastid ClpT1 and ClpT2 are plant-specific proteins that associate with the ClpPR protease. However, their physiological significance and structures are not understood. *Arabidopsis thaliana* loss-of-function single *clpt1* and *clpt2* mutants showed no visible phenotypes, whereas *clpt1 clpt2* double mutants showed delayed development, reduced plant growth, and virescent, serrated leaves but were viable and produced seed. The *clpt1* and *clpt1 clpt2* mutants showed partial destabilization of the ClpPR complex, whereas *clpt2* null mutants showed only marginal destabilization. Comparative proteomics of *clpt1 clpt2* plants showed a proteostasis phenotype similar to viable mutants in ClpPR core subunits, indicating reduced Clp protease capacity. In vivo and in vitro assays showed that ClpT1 and ClpT2 can independently interact with the single ClpP ring and ClpPR core, but not with the single ClpR ring. We determined ClpT1 and ClpT2 structures (2.4- and 2.0-Å resolution) and detailed the similarities to the N-domains of bacterial ClpA/C chaperones. The ClpT structures suggested a conserved MYFF motif for interaction with the ClpPR core near the interface between the P- and R-rings. In vivo complementation showed that ClpT function and ClpPR core stabilization require the MYFF motif. Several models are presented that may explain how ClpT1,2 contribute to ClpPR protease activity.

INTRODUCTION

The Clp protease system is the most abundant and complex serine-type protease in the soluble stromal phase of chloroplasts in *Arabidopsis thaliana* and likely most other higher plants (reviewed in Yu and Houry, 2007; Kato and Sakamoto, 2010; Olinares et al., 2011a; Nishimura and van Wijk, 2014; van Wijk, 2015). It consists of a 350-kD barrel-shaped ClpPR core complex formed by a heptameric ring with ClpP3, ClpP4, ClpP5, and ClpP6 (the P-ring) and a heptameric ring with ClpP1, ClpR1, ClpR2, ClpR3, and ClpR4 (the R-ring). Complementation of null mutants of *CLPR4* and *CLPP3* using StrepII-tagged versions of ClpR4 and ClpP3, respectively, allowed purification of individual ClpR and ClpP rings (Olinares et al., 2011b). By spiking these isolated P- and R-rings with stable isotope-labeled proteotypic peptides, the absolute stoichiometry of ClpPR subunits in each ring could be determined. This showed that the heptameric ClpR ring consists of ClpP1, R1, 2, 3, and 4 in a 3:1:1:1:1 ratio and that the P-ring consists of ClpP3, 4, 5, and 6 in a 1:2:3:1 ratio (Olinares et al., 2011b). The ClpPR core complex was initially observed by native gel electrophoresis in Arabidopsis chloroplasts and in nonphotosynthetic plastids of roots of *Brassica rapa* and flower petals of *Brassica oleracea* (Peltier et al., 2001, 2004). Moreover, native isoelectric focusing showed that the ClpPR core complex formed a single complex, rather than a mixture of ClpPR core complexes with different compositions (Peltier et al., 2004).

Mass spectrometry (MS) analysis and immunoblotting showed that the ClpPR core complex also contains copies of ClpT1 and ClpT2, two ~20-kD proteins with high sequence identity to the N-terminal domain of ClpA/C chaperones (reviewed in Nishimura and van Wijk, 2014). Image analysis of silver-stained and Coomassie blue-stained gels and titration experiments suggested that ClpPR core complexes contain on average one copy of each ClpT1 and ClpT2 (Peltier et al., 2004; Sjögren and Clarke, 2011). Homology modeling suggested that ClpT1 and ClpT2 are unlikely to be part of the ring structure, but rather associate with the axial side of the ClpP ring involving the so-called P1 pocket. ClpT proteins are not found in prokaryotes or nonphotosynthetic eukaryotes. Thus ClpT is specific for plastids in photosynthetic species and likely represents an adaptation to the plastid proteome and/or the Clp system (Peltier et al., 2004). Various hypotheses have been proposed for ClpT function: (1) selection of substrates, in particular those that do not require unfolding, such as cleaved chloroplast transit peptide (Peltier et al., 2004); (2) ClpPR complex assembly factors (Sjögren and Clarke, 2011); (3) tethering the association of other protein interactors, such as ClpS or Clp chaperones (Peltier et al., 2004); and, recently, (4) a regulator/stimulator of ClpC2 and ClpD chaperones (Colombo et al., 2014).

In an attempt to determine ClpT1,2 function, Arabidopsis single *CLPT* mutants (*clpt1-1* and *clpt2-1*) without visible growth phenotypes were analyzed (Sjögren and Clarke, 2011). Native gel electrophoresis indicated partial destabilization of the ClpPR core complex into the individual heptameric rings, in particular in

[1] Address correspondence to kv35@cornell.edu.
The author responsible for distribution of materials integral to the findings presented in this article in accordance with the policy described in the Instructions for Authors (www.plantcell.org) is: Klaas J. van Wijk (kv35@cornell.edu).
www.plantcell.org/cgi/doi/10.1105/tpc.15.00106

the *clpt1-1* mutants. No double mutants could be identified, and it was concluded that ClpT1 and ClpT2 are essential for ClpPR core assembly; hence, the double mutants would be embryo or seedling lethal (Sjögren and Clarke, 2011). However, as we will show and explain in this study, double mutants for ClpT1 (including with a stronger *clpt1-2* allele) and ClpT2 can be obtained, and they can complete their life cycle in soil, produce viable seed, and be maintained as a homozygous line. This viability allowed us to determine the ClpPR assembly state in single and double mutants and show that ClpT1,2 do contribute to ClpPR core stability, but that they are not strictly essential for ClpPR core stabilization/assembly. Perhaps even more interesting is that the strong growth phenotype of the double mutant cannot easily be explained by the partial ClpPR destabilization observed on native gels. In vivo protein interaction analysis that showed that ClpT1 and ClpT2 can independently interact with the intact core, but no support was found for interaction between ClpT1,T2 and ClpC chaperones, in contrast to a recent report in case of ClpT1 (Colombo et al., 2014). Comparative proteomics of *clpt1-2 clpt2-1* double mutants showed a molecular phenotype that shared several key features of mutants for the ClpPR subunits, *clpr2-1* (Rudella et al., 2006; Zybailov et al., 2009), *clpp3-1* (Kim et al., 2013), and *clpr4-1* (Kim et al., 2009). Following crystallization, structures for ClpT1 and ClpT2 were determined and compared with structural features to N-domains of bacterial Clp chaperones; the in vivo significance of two domains was tested. A functional model for ClpT1,2 is discussed.

RESULTS

Phylogeny of ClpT Proteins

The chloroplast ClpT proteins ClpT1 (At4g25370) and ClpT2 (At4g12060) show high sequence similarity (Supplemental Figure 1A) and are likely derived from ClpC chaperones given their significant sequence similarity (31% sequence identify across 93 to 98 residues) to the α-helical N-domain of chloroplast ClpC1,2 chaperones (see below). The N-domains in prokaryotic and plastid Clp chaperones contain two repeats and are involved in substrate binding and interaction with adaptor proteins (e.g., MecA, YpbH, and McsB for ClpC and ClpS for ClpA) in bacteria (Erbse et al., 2008; Kirstein et al., 2009; Kress et al., 2009; Striebel et al., 2009). To better understand ClpT proteins, we performed an in-depth phylogenetic analysis with two sequences from the moss *Physcomitrella patens* and 48 sequences from 31 vascular plants (41 sequences from 25 eudicots and seven sequences from six monocots). ClpT proteins in vascular plants clearly separated into two large clades, which we assigned ClpT1 and ClpT2 clades (Figure 1A; Supplemental Data Sets 1 and 2 provide full sequences and the sequence alignment used for generation of the cladogram). *P. patens* possesses two ClpT-like proteins, forming a separate clade (Figure 1A). All higher plants that we investigated contain ClpT1 and/or ClpT2 proteins. ClpT1 proteins were found in all higher plant species except *Medicago truncatula* and *Solanum tuberosum*, whereas some species contained two or three paralogs of ClpT1. ClpT1 sequences in monocots form a single subclade distinct from those in dicots. ClpT2 proteins are missing in all six monocots analyzed and are also missing in some dicots (*Cucumis sativus*, *Citrus sinensis*, *Ricinus communis*, and *Vitis vinifera*). The Brassicaceae form smaller subclades for each ClpT1 and ClpT2 (shown by five species in Figure 1A). Other proteins with homology to the N-domain Clp chaperone sequences have been found in the algae *Chlamydomonas* and *Volvox*, but not other algae; however, because they are so different from ClpT1 and ClpT2, these proteins were assigned as ClpT3 and ClpT4 (Derrien et al., 2012). It remains to be determined if these distant ClpT homologs have similar functions as ClpT1 and ClpT2. Some cyanobacteria also possess some N-domain-containing proteins that are not AAA^+ chaperones, but these are very distant from ClpT proteins in algae and plants (Derrien et al., 2012). Thus, ClpT1 and ClpT2 proteins are consistently present in higher plants, but not in cyanobacteria or algae, even if both cyanobacteria and green algae form heteromeric ClpPR complexes (see Nishimura and van Wijk, 2014). In the remainder of the article, we focus on the structure and function of ClpT1 and ClpT2 in Arabidopsis.

Accumulation of ClpPR Bound and Free ClpT1 and ClpT2

For understanding ClpT structure and function, it is important to know the N and C termini for ClpT, as well as the molar ratio between the ClpPR core complex and free and ClpPR-bound forms of ClpT1 and ClpT2. We note that both ClpT1 and ClpT2 each have only one predicted gene model (or splice form). MS analysis of stromal extracts and purified ClpPR core complexes identified the likely N termini of ClpT1 and ClpT2 (Supplemental Figure 1B). Mature ClpT1 protein starts with S65, whereas mature ClpT2 protein starts with S76. In the case of ClpT2, we also observe likely N-terminal peptides starting two residues downstream (Pro-78); such "ragged" N-terminal ends are quite common in the chloroplast proteome (E. Rowland and K.J. van Wijk, unpublished data). Projecting these N termini onto the sequence logos of 30 ClpT1 and 18 ClpT2 protein sequences from higher plants shows that these N termini coincide with a transition of lower sequence similarity to higher similarity (Supplemental Figure 2). This is consistent with the notion that cTPs are less conserved than the mature regions of protein homologs. Also, the C terminus is present in the mature ClpT1 and ClpT2 proteins without C-terminal trimming (Supplemental Figure 1B). Based on silver and Coomassie blue staining of stromal ClpPRT complexes, we previously estimated that ClpT1 and ClpT2 were present on average with one copy each per ClpPR core complex (Peltier et al., 2004). Extensive label-free spectral counting analysis of denatured chloroplast stromal proteomes by high-resolution tandem mass spectrometry (MS/MS) analysis also suggested an ~1:1 ratio between total ClpT1 and ClpT2 (Zybailov et al., 2008) and on average ~2.5 copies each of ClpT1 and ClpT2 per ClpPR core complex, when assuming that all ClpPR proteins are assembled in the tetradecameric core. We note that these latter experiments provide no information as to whether ClpT proteins are indeed associated to the ClpPR core. Based on spectral counting analysis of total

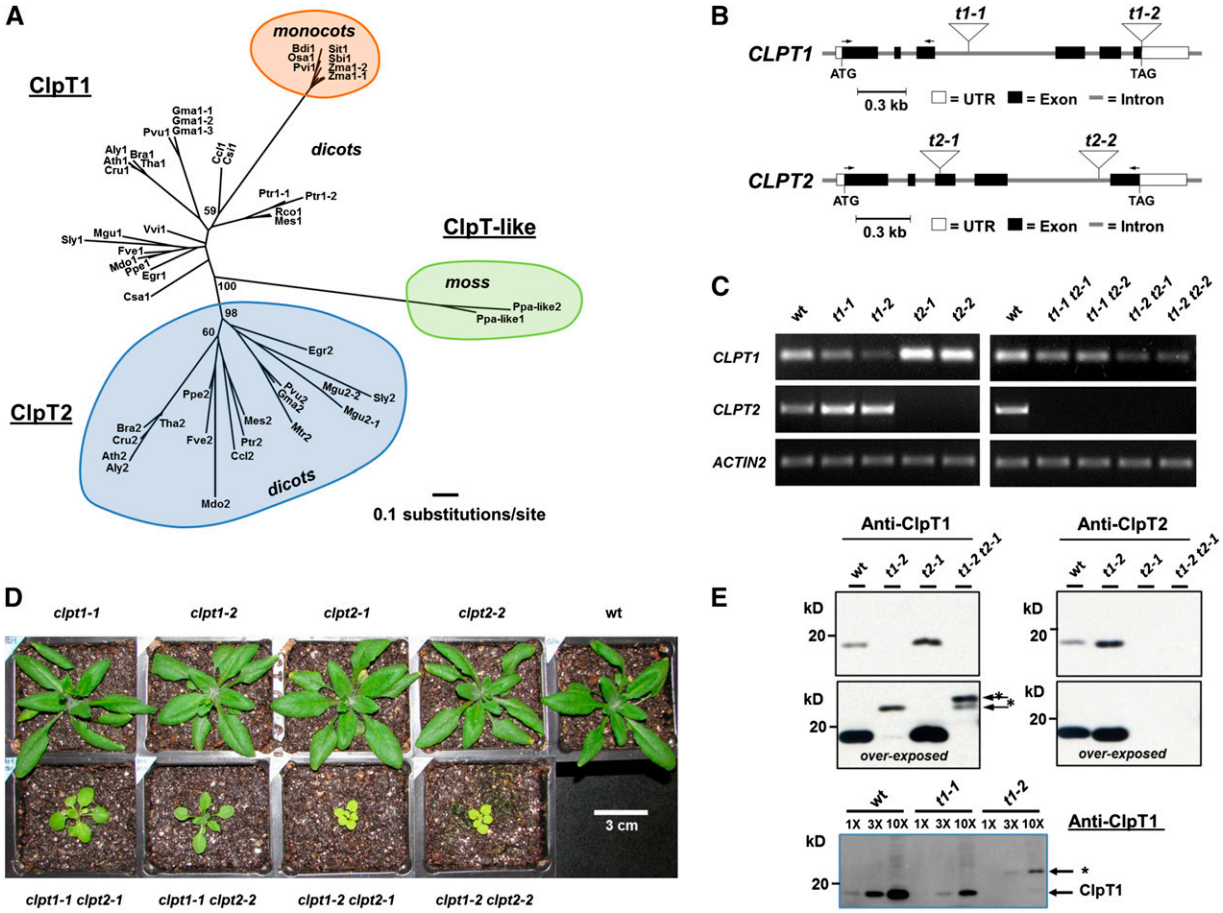

Figure 1. Phylogenetic Analysis of ClpT and Characterization of *clpt1* and *clpt2* Single and Double Mutants.

(A) Nonrooted phylogenetic tree of 50 ClpT proteins from six different monocots, 25 different dicots, and the moss *P. patens.* Bootstrap values are indicated for key branch points. Three main types or ClpT are assigned, namely, ClpT1 (both monocots and dicots), ClpT2 (only dicots), and ClpT-like protein in moss.

(B) Gene model structures and position of T-DNA inserts in the *CLPT* mutants used in this study. Exons (black boxes for coding sequence; open boxes for 5′ and 3′ untranslated regions [UTRs]) and T-DNA insertions (triangles) are indicated.

(C) Transcript accumulation levels in the leaves of the *CLPT* single and double mutants used in this study. Transcript levels were determined by RT-PCR (25 cycles) using gene-specific primer pairs; *ACTIN2* was used as internal control. At least three biological replicates were performed for each RT-PCR analysis (primers are listed in Supplemental Table 2).

(D) Growth and development of wild-type and homozygous *clpt* mutants grown on soil for 23 d under an 18/6-h light/dark cycle at 120 μmol photons m^{-2} s^{-1}. Bar = 3 cm.

(E) ClpT1 and ClpT2 protein levels in the single and double *clpt* mutants. Asterisks mark a protein recognized by the anti-ClpT1 serum. Ten micrograms of stromal protein was loaded in each lane for the upper panels. Total soluble protein was loaded in each lane for the lower panel. 1x, 3x, and 10x indicate that 3, 9, and 30 μg protein, respectively, was loaded.

wild-type leaf rosette denatured proteomes (after SDS-PAGE) with nine independent replicates, we estimate that the ClpPR subunits and the ClpT1 and ClpT2 subunits represent 0.36 and 0.08%, respectively, of the total leaf protein mass (Supplemental Table 1). Assuming that all ClpPR proteins are part of the ClpPR tetradecamer and correcting for the number of available tryptic peptides for quantification, this suggests an average approximately four copies of total ClpT1 and ClpT2 per ClpPR core (Supplemental Table 1). Thus, both stromal and total leaf proteome analysis suggest that there are four to five ClpT proteins for each ClpPR core, with comparable amounts of ClpT1 and ClpT2.

Growth and Developmental Phenotypes of CLPT1 and CLPT2 Single and Double Mutants

We screened the various T-DNA insertion collections in the Columbia-0 background for potential null and knockdown mutants in *CLPT1* and *CLPT2*. After extensive genotyping by PCR, DNA sequencing of the T-DNA inserts, and RT-PCR, we

identified two *CLPT1* mutants and two *CLPT2* mutants. The mutants are *clpt1-1* (SALK_052772), *clpt1-2* (GK_285A05), *clpt2-1* (SAIL_340A10), and *clpt2-2* (SALK_132943). The respective gene models and the position of the confirmed T-DNA insertions are shown in Figure 1B. RT-PCR of the homozygous *clpt2-1* and *clpt2-2* did not detect any *CLPT2* transcript, and they are thus null mutants. Transcript levels for *CLPT1* were 60 and 20% of wild-type levels in *clpt1-1* and *clpt1-2*, respectively (Figure 1C). Interestingly, transcript levels for *CLPT1* were about ~1.6-fold of wild-type levels in both *clpt2* alleles, and for *CLPT2* ~1.6-fold of wild-type levels in both *clpt1* alleles, indicative of a small transcriptional compensatory response (Figure 1C). The four homozygous alleles grown on soil were indistinguishable from wild-type plants (Figure 1D). Immunoblot analysis of leaf extract of both *clpt1* mutant alleles and *clpt2-1* showed that ClpT1 level was reduced to 25% in *clpt1-1* but was undetectable in *clpt1-2*, whereas ClpT2 was not detected in the *clpt2* mutant allele (Figure 1E). Interestingly, ClpT1 protein levels increased ~3-fold in *clpt2-1* and ClpT2 protein levels increased ~4-fold in *clpt1-2*, indicative of a strong compensatory response and suggesting (partial) functional redundancy between ClpT1 and ClpT2 (Figure 1E). When the anti-ClpT1 immunoblots were overexposed or when using higher protein loading, we observed a higher molecular mass band (~2 kD higher) specifically in the *clpt1-2* backgrounds (Figure 1E). Because the T-DNA insertion in *clpt1-2* was at the stop codon, we verified whether read-through translation could explain this higher mass band. Sequencing the genomic DNA for this allele showed loss of the original stop codon and a new stop codon 189 nucleotides downstream. RT-PCR of wild-type and *clpt1-2* cDNA indeed detected this longer transcript in the *clpt1-2* allele (Supplemental Figure 3). However, this should result in an additional 63 amino acids (~7 kD), which is much longer than the estimated protein size deduced from the anti-ClpT1 immunoblot (~2 kD increase). Therefore, it appears unlikely that the higher molecular mass band represents a read-through product. It should be noted that also in the *clpp3-1* null mutant a higher molecular mass form of ClpT1 (~1 kD higher) accumulates, but never ClpT2 (Kim et al., 2013). Despite significant efforts we have not been able to determine what the higher molecular mass bands represent.

To test the genetic interactions and possible functional redundancy between ClpT1 and ClpT2, we generated four different homozygous *clpt1 clpt2* double mutants using these *clpt1* and *clpt2* alleles. All four *clpt1 clpt2* mutant combinations showed delayed development, reduced growth and biomass, and a yellow to pale-green phenotype (Figure 1D). Consistent with the stronger reduction of ClpT1 expression, *clpt1-2 clpt2-1* and *clpt1-2 clpt2-2* plants showed more severe phenotypes than *clpt1-1 clpt2-1* and *clpt1-1 clpt2-2* plants (Figure 1D), illustrating a strong dosage effect of ClpT1. We did not detect phenotypic differences between the contributions of the two *clpt2* alleles, consistent with them both being null alleles. The *clpt1-2 clpt2-1* mutant could be fully complemented (no visible growth phenotype) with constructs that express either ClpT1 or ClpT2 (both StrepII-tagged) (Supplemental Figures 4A and 4B), indicating that ClpT1 and ClpT2 are at least partially redundant. Immunoblot analysis of leaf extracts of *clpt1-2 clpt2-1* plants did not detect ClpT1 or ClpT2 protein, except for two higher mass molecular bands in case of ClpT1 at ~2 to 2.5 kD (Figure 1E). One band aligned to the higher mass band observed in the *clpt1-2* single mutant, whereas the other was slightly higher in mass (Figure 1E). MS/MS analysis of total leaf extracts of *clpt1-2 clpt2-1* mutants neither detected ClpT1 nor ClpT2, whereas ClpT1 and ClpT2 were detected with high confidence in the wild-type plants (Supplemental Data Set 3). A developmental series of *clpt1-2 clpt2-1* plants is shown in Supplemental Figure 4C. The *clpt1-2 clpt2-1* double mutant was smaller in stature (20 to 30% in rosette cross section) as the leaky *clpr2-1* mutant with ~20% ClpR2 levels conditions (Rudella et al., 2006), but leaf color and shape were very similar (Supplemental Figures 4D and 4E). Size differences were greater under short-day than long-day conditions. However, the phenotype of the *clpt1-2 clpt2-1* double mutant was much weaker than null mutants for *CLPP3* and *CLPR4* (both arrested in development in the cotyledon stage) and the embryo-lethal *CLPP4* and *CLPP5* null mutants; this is summarized in Figure 2A. In the remainder of the article, we use the stronger *CLPT1* allele (*clpt1-2*), rather than the weaker allele (*clpt1-1*) for further analysis.

Molecular Phenotyping of *clpt1-2 clpt2-1* by Comparative Proteomics

To gain insight in the consequences of the loss of ClpT1 and ClpT2, we compared the total denatured leaf proteomes of the *clpt1-2 clpt2-1* double mutant and wild-type plants in developmental stage 1.11 (Figure 2B). Total leaf proteomes were extracted with SDS, and each proteome was separated by SDS-PAGE, followed by in-gel trypsin digestion, protein identification, and quantification by nano-liquid chromatography-MS/MS, resulting in the identification of 2360 proteins, quantified as 1775 individual proteins and 126 protein groups (Supplemental Figures 5A and 5B and Supplemental Data Set 3). The average pairwise correlation coefficients among the three biological replicates within the wild-type and *clpt1 clpt2* data sets were 0.937 and 0.968, respectively, indicating high reproducibility between the independent replicates for each genotype (Supplemental Figure 5C). Principle component analysis also showed that the variation between genotypes was larger than between replicates within each genotype (Figure 2C). Together, this shows that the quantitative proteome data are of high quality with little noise and that the *clpt1-2 clpt2-1* mutant has a measurable proteome phenotype. Based on our recent reference Arabidopsis chloroplast proteome (Huang et al., 2013) and additional updates, 795 proteins were chloroplast localized (including 38 dual localized proteins), representing 56% of the protein mass in the double mutant and 59% in the wild type. Compared with the wild type, the *clpt1-2 clpt2-1* thylakoid proteome mass decreased by 23%, but the proteome mass of thylakoid-associated plastoglobuli (Lundquist et al., 2012) (20 identified proteins) more than doubled (2.35-fold higher), reflecting loss of photosynthetic electron transport capacity and increased thylakoid stress. Statistical analysis using the consensus results of two different statistical packages (GLEE with $P < 0.01$ and QSPEC at false discovery rate < 0.05; see Methods) showed that among the 51 significantly changed proteins in

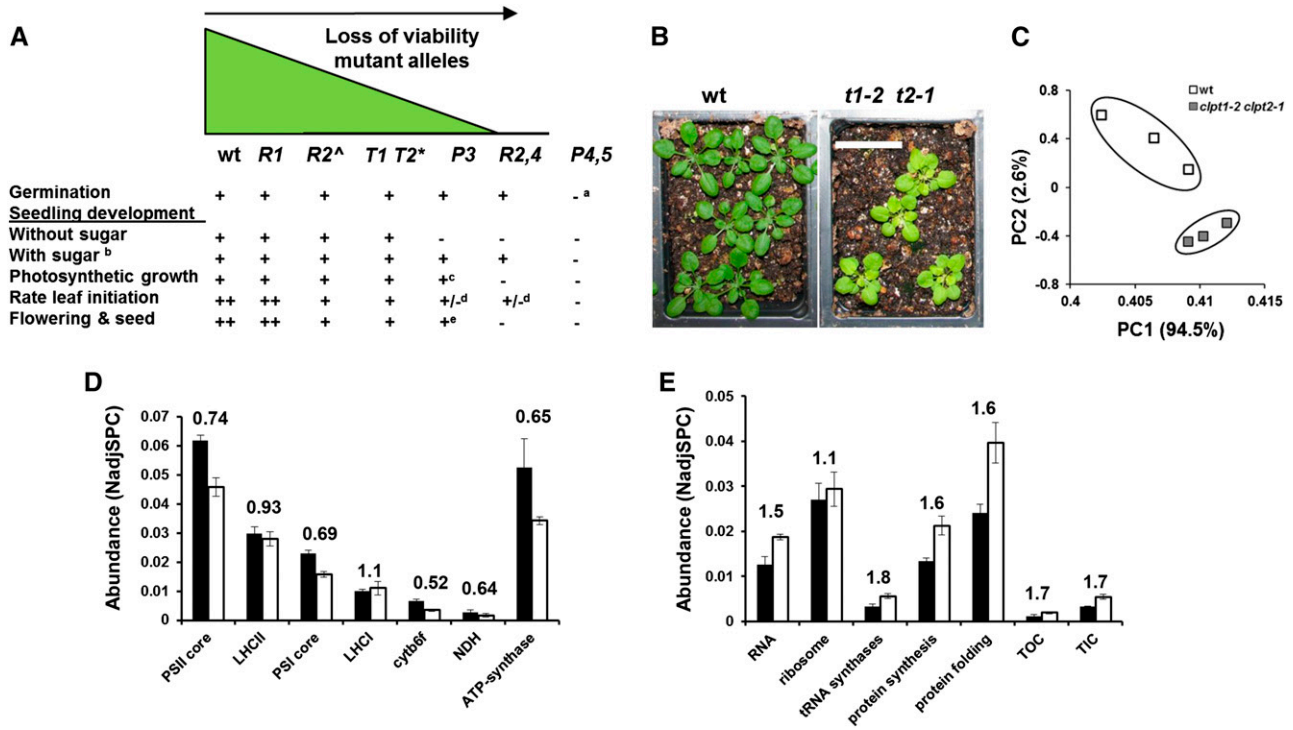

Figure 2. Comparison of *clp* Mutants and Comparative Proteomics of *clpt1-2 clpt2-1* and the Wild Type.

(A) Summary of phenotypes of CLPPRT mutants. ^, *clpr2-1* leaky allele with ~20% mRNA and protein. *, *clpt1-2 clpt2-1*. [a], Nomarski microscopy shows an early block in embryogenesis (no abortion); [b], sugars can be sucrose or glucose (1 to 3%); [c], after initial growth on sugar-containing medium; [d], requires sugar in the medium; [e], strongly delayed flowering.

(B) The *clpt1-2 clpt2-1* and wild-type (wt) plants used for proteome analysis. Total leaves were harvested at growth stage 1.11, 41 d for *clpt1-2 clpt2-1* and 27 d for the wild type. Plants were grown on soil under a short-day cycle (10-h/14-h light/dark) at 100 μmol photons m^{-2} s^{-1}. The Coomassie blue-stained SDS-PAGE gel with extracted proteomes is shown in Supplemental Figure 5A.

(C) Principal component analysis based on NadjSPC of individual replicates for the wild type and double mutant.

(D) and **(E)** Figures illustrating the molecular proteome phenotype of the thylakoid photosynthetic machinery **(D)** and plastid gene expression and proteotasis **(E)**. Black bars indicate the wild type, and open bars represent *clpt1-2 clpt2-1* plants.

clpt1-2 clpt2-1 leaves, chloroplast proteins were overrepresented (37/51), consistent with the location of the Clp system. Significantly changed extraplastidic proteins were located in different subcellular compartments and did not show any specific functional trends.

Evaluation of the *clpt1-2 clpt2-1* functional chloroplast proteome phenotype suggests particular bottlenecks or defects in protein import, chloroplast translation, protein folding stress, and loss of photosynthetic capacity (Table 1, Figures 2D and 2E). Below, we highlight the most interesting aspects of the *clpt1-2 clpt2-1* chloroplast proteome phenotype.

Loss of Photosynthetic Capacity

Relative protein mass investments in the photosynthetic electron transport chain and Calvin cycle decreased very similarly by 24 and 22%, respectively. Within the thylakoid-bound photosynthetic apparatus, the photosystem II core, photosystem I core, the cytochrome b_6f complex, the NDH complex, and the ATP-synthase decreased by 26, 31, 48, 36, and 35%, whereas light-harvesting complex II (LHCII) and LHCI did not significantly change (Figure 2D). Also in the other Clp core mutants, the downregulation of LHCs is much less than for the photosystem I and photosystem II cores or other thylakoid complexes (Supplemental Figure 5D).

Protein Synthesis and Folding Stress

Protein translation initiation and elongation factors together increased by 59% and tRNA synthases increased by 75%, whereas ribosome protein mass increased by just 9% (Figure 2E). Stromal protein chaperones (e.g., CPN60, HSP70, and HSP90), isomerases (e.g., ROC4), and the unfoldase ClpB3 increased collectively by 73% (Figure 2E). Within these functions, several individual proteins significantly increased, in particular, the chaperones and three elongation factors (Table 1).

Protein Import Bottleneck

The abundance level of the chloroplast envelope TOC and TIC protein import apparatus increased by 65 and 69%, respectively, indicative of a bottleneck in protein import (Figure 2E).

Table 1. Chloroplast Proteins Significantly Up- or Downregulated in *clpt1-2 clpt2-1* Compared with the Wild Type and Comparison to ClpPR Core and ClpC1 Mutants

Best Model	Protein Annotation	Function	Total adjSPC[a]	*clpt1xclpt2*/ Wild Type[a]	*clpr2-1*/ Wild Type[b]	*clpp3*/ Wild Type[c]	*clpc1-1*/ Wild Type[d]
AT1G06950.1	Tic110	Protein import	280	1.6	3.6	2.1	[ND in mutant]
ATCG01130.1	Tic214 (YCF1.2)	Protein import	32	12.1 (#)	[ND]	[ND in wild type]	[ND]
AT1G55490.1 AT3G13470.1	Cpn60-β-1,2	Protein folding	708	1.9	2.4**	2.2	[1.7]
AT5G56500.1	Cpn60-β-3	Protein folding	64	5.4	2.4**	8.3	ND in wild type
AT2G28000.1	Cpn60-α-1	Protein folding	656	1.8	2.2	2.1	[1.4]
AT4G24280.1	cpHSP70-1	Protein folding	213	1.8	2.0	2.5	[1.0]
AT5G49910.1	cpHSP70-2	Protein folding	187	2.0	3.2	2.5	[1.1]
AT2G04030.1	cpHSP90	Protein folding	232	1.9	2.3	2.4	[1.6]
AT5G15450.1	ClpB3	Protein unfolding	52	3.3	6.6	5.5	3.4
AT3G62030.1	Peptidylprolyl isomerase (ROC4; CYP20-3)	Protein folding	312	1.4	2.3	1.5	[0.8]
AT4G12060.1	ClpT2	Clp system	31	ND in mutant	[2.2]	[1.9]	[1.4]
AT4G25370.1	ClpT1	Clp system	20	ND in mutant	[2.8]	[1.7]	2.1
AT3G19170.1	Prep1-Zn metalloprotease	Peptidases	310	1.6	4.2	2.4	[1.4]
AT5G42390.1	Stromal processing peptidase (SPP)	Peptidases	74	2.4	[ND]	5.5	[1.6]
AT5G26742.2	DEAD box RNA helicase (RH3)	RNA splicing	124	2.7	8.0	2.4	[ND]
AT4G16390.1	PPR protein P67 (SVR7)	RNA metabolism	29	ND in wild type	[ND]	3.8	[1.0]
AT1G70070.1	DEAD/DEAH box helicase	RNA metabolism	29	ND in wild type	[ND]	4.0	[2.0]
AT4G20360.1	Elongation factor Tu (EF-Tu-1), plastid	Protein synthesis	703	1.7	1.5	1.7	[1.6]
AT5G13650.1	Elongation factor typeA/bipA-like (SVR3)	Protein synthesis	111	3.1	4.6	3.5	2.7
AT1G62750.1	Elongation factor Tu-G (EF-G; SCO1)	Protein synthesis	387	1.4	[2.0]	2.3	[1.5]
AT3G26650.1	Glyceraldehyde 3-phosphate dehydrogenase A-1 (GAPA-1)	Calvin cycle	432	0.5	[0.9]*	[0.9]	0.4
AT5G38420.1 AT5G38410.1	Rubisco small subunit 2b/3b	Calvin cycle	397	0.5	[1.0]*	0.4	0.6
AT5G60600.1	4-Hydroxy-3-methylbutyl diphosphate synthase (HDS; also GcpE, CLB4, IspG)	MEP pathway	147	3.2	10.6	3.2	2.1
AT1G69740.1	δ-Aminolevulinic acid dehydratase-1 (ALAD-1)	Tetrapyrrole synthesis	66	3.0	[1.7]	[1.94]	1.6
AT5G53460.1	NADH-GOGAT or NADH-glutamate synthase (GLT1)	N-metabolism	215	5.6	1.6	21.9	3.2
AT4G31990.1	Aspartate aminotransferase (AAT1; Asp5)	Amino acid metabolism	130	2.0	[1.2]	2.8	[0.7]
AT3G11630.1	2-Cys Peroxiredoxin A (Prx A)	Redox and stress	155	2.0	[1.4]	[1.4]	[0.9]
AT1G76080.1	Thioredoxin (CDSP32)	Redox and stress	42	3.7	[3.0]	[2.0]	[1.2]
AT3G26060.1	Lumenal peroxiredoxin Q (Prx Q)	Redox and stress	72	0.3	[0.9]	0.3	[1.6]
AT4G04020.1	Fibrillin 1a (FBN1a)	Plastoglobules	123	2.6	4.0	4.3	ND in wild type
AT4G22240.1	Fibrillin 1b (FBN1b)	Plastoglobules	62	5.3	5.8	15.5	ND in wild type

Single asterisk indicates that ratios are significantly decreased at stage 1.07. Double asterisks indicate group with Cpn60-β1,2,3. #, This ratio is artificially high due because YCF1 was only observed once in the wild type (two missing values) and one high outlier value in the mutant. ND, not detected.

[a]Protein abundance ratio for *clpt1-2 clpt2-1*/wild type (growth stage 1.11; this study). Statistically significant changes. AdjSPC, number matched adjusted MS/MS spectra across all replicates and both genotypes.

[b]Protein abundance ratio for *clpr2-1*/wild type (average growth stage 1.07 and 1.14; from Zybailov et al., 2009). Statistically significant changes. Protein ratios in brackets are not significantly changed.

[c]Protein abundance ratio for *clpp3-1*/wild type (growth stage 1.14; from Kim et al., 2009). Statistically significant changes. Protein ratios in brackets are not significantly changed.

[d]Protein abundance ratio for *clpc1-1*/wild type (average growth stage 1.08 to 1.09; from Nishimura et al., 2013). Statistically significant changes. Protein ratios in brackets are not significantly changed.

Feedback on Chloroplast Proteases

The abundances of the ClpP ring, the ClpR ring, and ClpC1 and ClpC2 were not significantly changed, whereas stromal peptidases SPP (Teixeira and Glaser, 2013) and PREP1 (Kmiec et al., 2014) both significantly increased by 136 and 59%, respectively (Table 1). Other relatively abundant stromal proteases, such as peptidases CGEP (Forsberg et al., 2005), OOP (Kmiec et al., 2013), and DEG2 (Schuhmann and Adamska, 2012), did not significantly change in *clpt1-2 clpt2-1* mutants. The thylakoid FTSH heterooligomeric complex (FTSH1,2,5,8) decreased by 16%, but after normalization for thylakoid protein mass, thylakoid FTSH was increased by 9%. The lack of significant increase in thylakoid FTSH capacity was also observed in other Clp core mutants (Kim et al., 2013).

No Differential Effect on Chloroplast-Encoded Compared with Nuclear-Encoded Proteins, Despite Significant Increase in Chloroplast Elongation Factors

The Arabidopsis chloroplast genome contains 79 genes; most of these code for ribosomal subunits (26 proteins) or thylakoid proteins of the photosynthetic apparatus (43 proteins). Because ribosomes and the thylakoid photosynthetic apparatus also contain many nuclear-encoded proteins, we determined if nuclear-encoded and chloroplast-encoded proteins were differentially affected within each of these two main functions. Chloroplast-encoded and nuclear-encoded ribosomal proteins increased by 19 and 6%, respectively, but this difference was not significant. Chloroplast-encoded and nuclear-encoded thylakoid photosynthetic proteins decreased by 30 and 17%, respectively, but this differential response was due to the lack of decrease in LHC proteins (all nuclear-encoded) and is not related to nuclear versus chloroplast gene expression. This can be illustrated by the comparison between chloroplast-encoded and nuclear-encoded proteins within photosystem II core; these were 23 and 33% downregulated, respectively, in the mutant. In summary, the *clpt1 clpt2* mutant shows no systematic differential effect on the levels of chloroplast-encoded versus nuclear-encoded proteins within the same function or complex. Moreover, chloroplast-encoded proteins were clearly not affected in the same manner (e.g., ribosomal proteins levels are barely changed while thylakoid proteins are strongly downregulated), suggesting that despite the strong increase in protein translation factors and tRNA synthases, plastid gene expression was not systematically affected.

Direct comparison of the significantly changed plastid proteins with significantly changed chloroplast proteins in *CLPPR* core and *CLPC1* mutants (Rudella et al., 2006; Kim et al., 2009, 2013; Zybailov et al., 2009; Nishimura et al., 2013) showed great consistency as is illustrated in Table 1. This suggests that the *clpt1-2 clpt2-1* molecular phenotype results mainly from reduced Clp protease capacity (see Discussion).

Assembly State of the ClpPR Core Complex in the *CLPT* Single and Double Mutants

The ClpPR core complex consists of a ClpP and a ClpR ring, as demonstrated extensively in previous studies (reviewed in Nishimura and van Wijk, 2014). Most of the ClpPR complex is stable when analyzed by one-dimensional native gel electrophoresis (1D-BN-PAGE) and migrates as a single 350-kD complex, but destabilization (between the P- and R-ring but not within the rings) can occur during the protein isolation and/or electrophoresis process. Indeed, complete dissociation of the ClpPR core into individual, intact P- and R-rings can be obtained by incubation with NaCl in the absence of stabilizers such as glycerol (Olinares et al., 2011b; Derrien et al., 2012). To determine the consequences of the loss of ClpT1 and/or ClpT2 on the stability/assembly state of the ClpPR core complex, chloroplast stromal proteomes of the wild type, *clpt1-2*, *clpt2-1*, and *clpt1-2 clpt2-1* were extracted under nondenaturing conditions and proteins were separated by 1D-BN-PAGE, followed by immunoblotting with specific antisera against ClpP6 and ClpP4 (as representatives of the P-ring) and ClpR2 (as representative of the R-ring). This showed that in the wild type, indeed, ~70 to 90% of the ClpPR proteins accumulated in the 350-kD complex with the remainder accumulating in ~200-kD heptameric ClpP or ClpR rings (Figure 3A). In contrast, in both *clpt1-2* and *clpt1-2 clpt2-1*, the ClpPR complex was partially destabilized and only ~20 to 30% of the ClpPR subunits were found in the 350-kD complex, with the remainder in the individual P- and R-rings. However, most of the ClpPR core (60 to 70%) remained stable in *clpt2-1* (Figure 3A). This shows that (1) ClpT1 is more important in the stabilization of the ClpPR core than ClpT2 and, surprisingly, that (2) loss of both ClpT1 and ClpT2 leads to similar levels of destabilization as loss of only ClpT1, despite the much stronger phenotype of the double mutants compared with the single mutants. This immediately suggests that the observed destabilization on the native gels cannot be the only causative effect of the strong developmental and growth phenotype of the *clpt1 clpt2* double mutants. Consequently, ClpT1 and ClpT2 must have a function in addition to stabilizing the interactions between the ClpP and ClpR rings (as visualized by native gels), such as activation through structural changes within the core (see Discussion).

To quantify the association of ClpT1 and ClpT2 to the ClpPR core, the 1D-BN-PAGE lanes for the wild type and the double mutant were directly transferred to membranes and immunoblotted with anti-T1 and anti-T2 (Figure 3A), or the native gels lanes were first denatured and proteins separated in the second dimension by SDS-PAGE, followed by immunoblotting with anti-ClpT1 and anti-ClpT2 (Figure 3B). In the case of the wild-type plants, this showed that both ClpT1 and ClpT2 were found in the 350-kD complex, as well as in a low molecular mass free form. Relatively more of ClpT1 than of ClpT2 was associated with the core complex. In *clpt1-2* and the double mutant, ClpT1 was detected at ~20% of wild-type levels, indicating that there is indeed a low level of residual ClpT1 in *clpt1-2* backgrounds and that this ClpT1 does associate with the ClpPR core and Clp ring. The ClpT1 signal was a bit stronger in the double mutant than the *clpt1-2* mutant, consistent with the immunoblot shown in Figure 1E.

To test if addition of ClpT1 and/or ClpT2 to the *clpt1-2 clpt2-1* mutant stimulated ClpPR core assembly/stability, we overexpressed and purified ClpT1 and ClpT2 from *Escherichia coli* (designated rClpT1 and rClpT2). Stroma from *clpt1-2 clpt2-1*

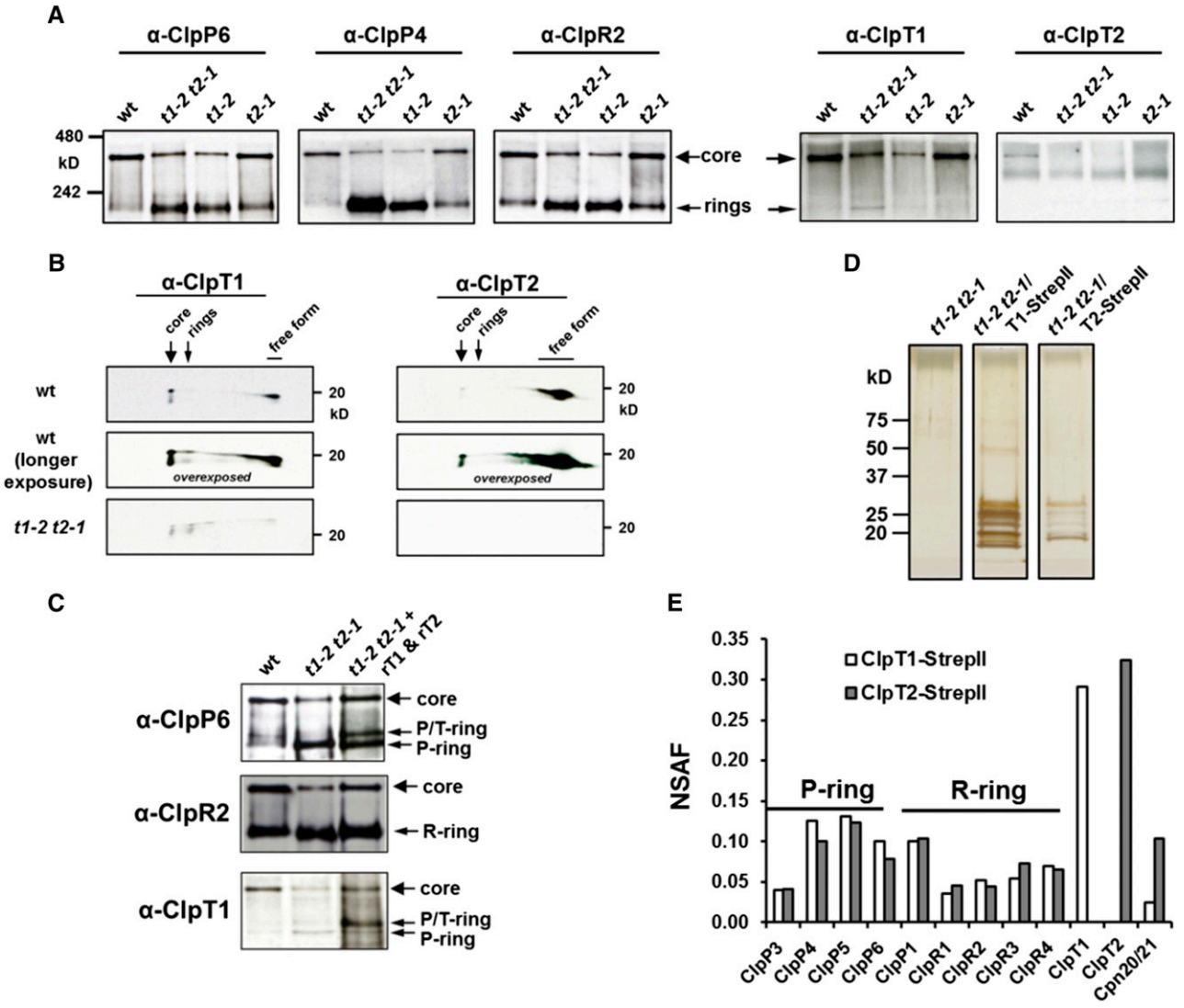

Figure 3. Assembly State of the ClpPRT Proteins and ClpT Interactions.

(A) Immunoblot analysis after native gel electrophoresis to visualize the Clp core assembly state. Stromal proteins obtained from isolated chloroplasts from the wild type (wt), *clpt1-2 clpt2-1*, *clpt1-2*, and *clpt2-1* plants were separated on native gels, transferred to blots, and probed with antisera against ClpP6, ClpP4, ClpR2, ClpT1, and ClpT2. The larger arrows indicate ClpPRT core complexes (350 to 400 kD), while the smaller arrows indicate Clp complexes between 180 and 240 kD, corresponding to heptameric ClpPR rings. Thirty micrograms of stromal protein was loaded in each lane.
(B) Immunoblot analysis after 2D electrophoresis. Protein complexes from the wild type and the *clpt1-2 clpt2-1* double mutant were separated as in **(A)** by BN-PAGE (first dimension) followed by SDS-PAGE (second dimension). The 2D gel separated proteins were transferred to blots and probed with antisera against ClpT1 and ClpT2. The positions of detected ClpPRT core, ClpP and ClpR rings, and free ClpT forms are indicated.
(C) Testing the assembly state of the ClpPR core in *clpt1-2 clpt2-1* extracts, following addition of recombinant ClpT proteins. Stromal proteins were obtained from isolated chloroplasts from wild-type and *clpt1-2 clpt2-1* plants. Recombinant ClpT1 and ClpT2 proteins (0.3% mass of total stromal protein mass) were added to the *clpt1-2 clpt2-1* stromal proteins and incubated at 22°C for 3 min. The mixtures were then separated on native gels, transferred to blots, and probed with antisera against ClpP6, ClpR2, and ClpT1. The larger arrows indicate ClpPRT core complexes (350 to 400 kD), while the smaller arrows indicate ClpP/T-ring, P-ring, or R-ring.
(D) SDS-PAGE analysis of affinity-purified *CLPT1*-StrepII and *CLPT2*-StrepII-tagged proteins. Isolated stromal protein from wild-type and transgenic plants was loaded on a Strep-tactin column and elutes were loaded. SDS-PAGE gel was silver stained.
(E) Relative abundance of ClpT1 and ClpT2 interacting proteins as determined by MS from gel bands in **(D)**. NSAF is the normalized spectral abundance factor, which is a measure of protein abundance normalized for protein length (Zybailov et al., 2008). More information is provided in Table 2.

was incubated with rClpT1 and rClpT2, and extracts were subsequently run on 1D-BN-PAGE, transferred to blots, and probed with antisera against ClpP6 (representing the P-ring), ClpR2 (representing the R-ring), and ClpT1 (Figure 3C). This resulted in an increase of the ClpPR core and accumulation of a ClpP ring with associated rClpT, but never a ClpR ring with associated rClpT. Thus, exogenous ClpT can help to stabilize the ClpPR core complex in 1D-BN-PAGE.

ClpT1- and ClpT2-Interacting Proteins

To determine if proteins other than the ClpPR core interact with ClpT1 or ClpT2 and to determine if ClpT1 and ClpT2 can interact with the ClpPR core independently of each other, we generated transgenic Arabidopsis lines expressing StrepII-tagged ClpT1 or ClpT2 subunits in the *clpt1-2 clpt2-1* double homozygous mutant background. The eight-residue StrepII tag (Schmidt and Skerra, 2007) was attached to the C terminus rather than the N terminus to prevent interference with the N-terminal chloroplast targeting peptide. Previously we used StrepII-tagged ClpR4 and ClpP3 lines successfully to purify ClpPR cores (Olinares et al., 2011b). The StrepII-tagged ClpT1 and ClpT2 lines grew well on soil and, in contrast to the *clpt1-2 clpt2-1* line, exhibited wild-type-like phenotypes (Supplemental Figure 4A). PCR of genomic DNA (data not shown) and immunoblotting using an anti-StrepII antibody confirmed the complementation (Supplemental Figure 4B). For affinity purification, chloroplast stromal proteins were isolated from the *CLPT1*-StrepII and *CLPT2*-StrepII-tagged complemented lines, as well as from the *clpt1-2 clpt2-1* double homozygous line serving as negative control. After affinity purification using Strep-Tactin superflow columns, protein eluates were run on an SDS-PAGE gel and then stained with silver nitrate (Figure 4D). MS analyses of the gel bands identified all nine ClpP and ClpR subunits, as well as the StrepII-tagged baits in both *CLPT1*-StrepII and *CLPT2*-StrepII complemented lines; none of these Clp proteins were present in the negative control (Figure 3E). Importantly, this shows that ClpT1 and ClpT2 can each independently interact with the ClpPR core. Whereas the ClpT2-StrepII purification overall yielded less MS/MS spectra, the ratio of matched MS/MS spectra for the ClpPR subunits per ClpT was the same for ClpT1-StrepII and ClpT2-StrepII (Supplemental Table 3). We also note that the P-ring and R-ring subunits were present in a roughly equal ratio, indicating that we purified mostly intact ClpPR cores (Figure 3E). We identified one additional candidate interacting protein, namely, the cochaperonin CPN20 (AT5G20720) (Koumoto et al., 1999). This protein was present with a significant number of MS/MS spectra in both ClpT1 and ClpT2 StrepII purifications but not in the negative controls (Table 2). In previous experiments, extensive StrepII purification of the ClpPR core using complemented null mutants for *CLPP3* and *CLPR4* with StrepII-tagged ClpP3 and ClpR4 proteins (Olinares et al., 2011b), we found either very low levels or no CPN20 in these StrepII purifications, indicating that CPN20 enrichment is not a common, unspecific interactor in StrepII affinity purifications and/or a direct interactor with the ClpPR rings. Finally, it was recently reported that ClpT interacts with ClpC2 and ClpD chaperones and stimulates ClpD chaperone activity (Colombo et al., 2014). However, our StrepII-tagged ClpT1/2 purification did not identify ClpC/D chaperones as interacting proteins.

ClpT Structure Determination

ClpT1 and T2 are unique to higher plants and their interaction with the ClpPR core (and perhaps other proteins) likely represents a specific adaptation to the plastid proteome and/or higher plant plastid Clp protease system. In order to gain functional understanding of ClpT1 and ClpT2 and how they might interact with the ClpP ring, we determined their structures by x-ray crystallography. We crystallized a ClpT1 (S65-Q238) and a ClpT2 (S76-E241) construct representing the mature proteins and determined their structures at a resolution of 2.4 and 2.0 Å, respectively (Figure 4A, Table 2). Both structures had two monomers per asymmetric unit; the two independent chains (molecules) in the ClpT1 structure can be superimposed with a root mean square deviation (r.m.s.d.) of 0.21 Å, while those of ClpT2 can be superposed with an r.m.s.d. of 0.25 Å, implying minimal difference between chains. (Note: ClpT1 and ClpT2 have differing numbering due to differing lengths of the cTP; equivalent numbering for mature ClpT2 can be derived from ClpT1 by adding 8 starting with Lys-90 in ClpT2 [Supplemental Figure 1A].)

The structure of each ClpT paralog is organized around a set of eight α-helices, which show a clear internal repeat organization where helices αA to αD (repeat 1 in the N-domain) are structurally equivalent to helices αE to αH (repeat 2 in the N-domain) (Figure 4A). The ClpT1 and ClpT2 structures closely resemble one another and can be superimposed with an r.m.s.d. of 0.55 Å (Figure 4B). Because they are very similar, in the following discussion, we focus on the more complete and better resolved ClpT2 structure (Figure 4A), pointing out differences in ClpT1 where pertinent. Searching the Protein Data Bank (http://www.rcsb.org/pdb/) with ClpT2 in PDBeFold shows that these proteins are most closely related to the N-terminal domain of *Bacillus subtilis* ClpC (2y1r), with r.m.s.d. of 1.57 Å over 137 residues (Wang et al., 2011); this structural similarity reinforces the idea that ClpT may be derived from the bacterial ClpC N-domain. The bacterial protein cg2963 from *Corynebacterium glutamicum* is also structurally closely related (3fh2; 1.82 Å over 137 residues), as well as the N-terminal domains of *E. coli* ClpB (1khy; 2.2 Å over 133 residues) and the N-terminal domain of *E. coli* ClpA (1r6q; 2.37 Å over 128 residues) (Xia et al., 2004). Figure 4C (and Supplemental Figure 5A) shows the overlay between the structures of ClpT1, ClpT2, and N-domains of *B. subtilis* ClpC (2y1r) and *E. coli* ClpA (1r6q).

Candidate Binding Sites of ClpT

Studies of complexes formed by homologous Clp N-domain structures, including *E. coli* ClpA, *B. subtilis* ClpC, and *Vibrio cholera* ClpV, show that at least four independent surfaces in the N-domain structures are utilized to recognize (different) binding partners. The most commonly utilized site is centered on the convergence of the N-terminal ends of helix αB, αE, and αG (Supplemental Figure 6B). Here, the amide nitrogen atoms at the N-terminal end of αB coordinate with two conserved threonine

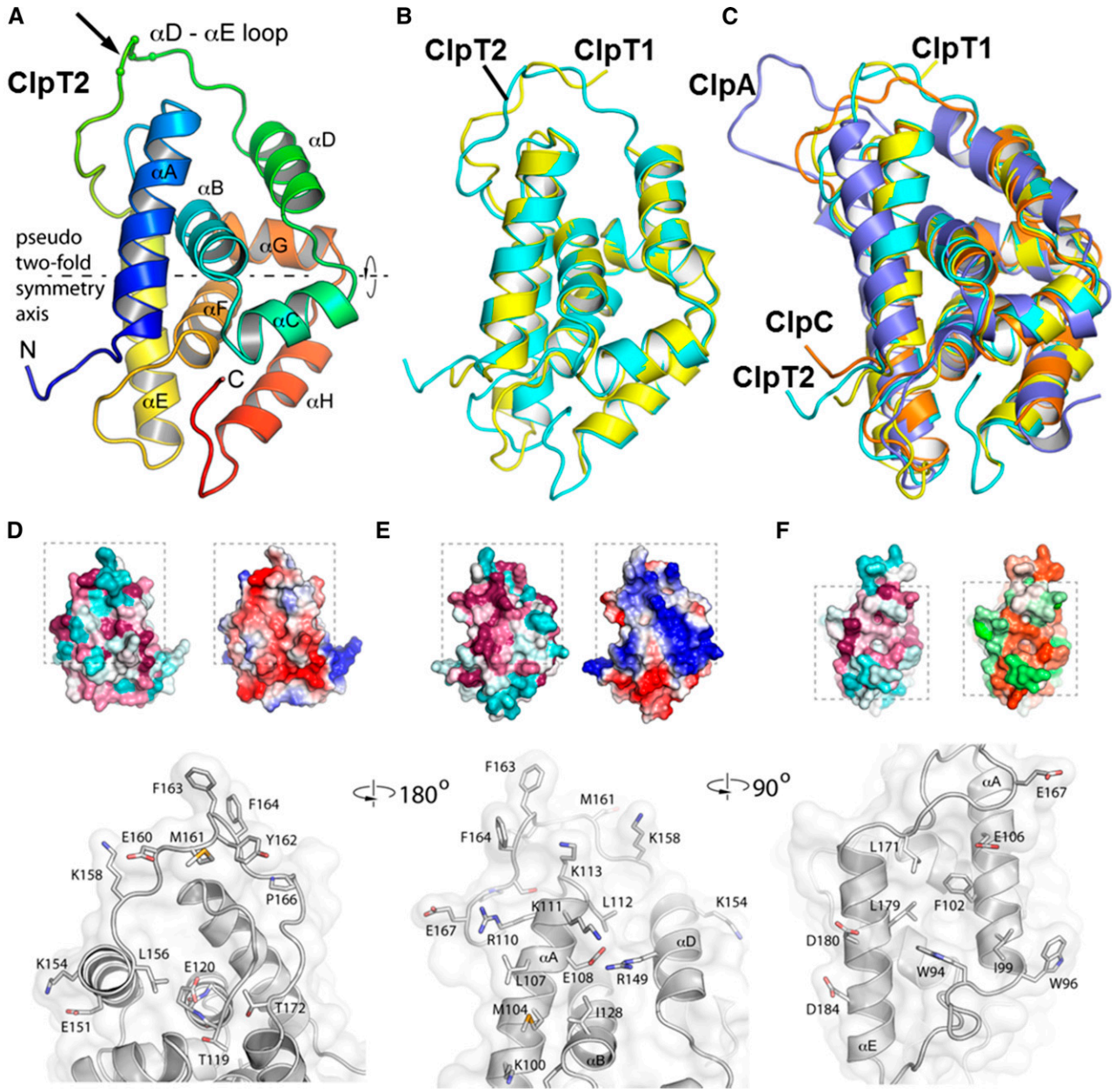

Figure 4. Structural Information on ClpT1 and ClpT2 and Docking to the ClpP Ring.

(A) ClpT2 monomeric structure, colored in a gradient of blue to red (blue-green-yellow-orange-red) from the N to C terminus. This view is oriented to show the pseudo 2-fold symmetry that here lies horizontal in the plane; 68 residues of the two related halves of ClpT2 can be superimposed with a 2.6-Å r.m.s.d. and are 15% identical at the sequence level. For ClpT1, 64 residues can be superposed with a 2.1-Å r.m.s.d. and are 22% identical. In ClpT2, the region (22 amino acids) N-terminal of Lys-93 in ClpT2 (corresponding to Lys-85 in ClpT1) is disordered in chain B, while in chain A, residues N-terminal to Lys-90 are disordered, except residues Ser-76 to Asn-81, which are weakly stabilized by crystal packing interactions; therefore, these N-terminal ClpT2 regions are not displayed. The position of the MYFF motif in the αD-αE loop is marked with small spheres (marked with an arrow).
(B) Superposition of ClpT paralogs. ClpT1 is shown in yellow and ClpT2 in cyan. These structures superpose closely, with the main differences in the αD-αE loop, and the disorder of the C terminus in ClpT1. In the ClpT1 structure, residues N-terminal to Pro-84 (14 residues) and C-terminal to Glu-227 (11 residues) are disordered in both chains and are therefore not displayed.
(C) Superposition of ClpT homologs. ClpT1 is shown in yellow, ClpT2 in cyan, *E. coli* ClpA N-terminal domain in blue, and *B. subtilis* ClpC N-terminal domain in orange. Note that despite the general organizational similarity of these proteins, differences in the positions of individual helices and long connecting loops can result in very different interaction surfaces.
(D) to **(F)** Three conserved interaction surfaces in ClpT2. The upper left insets show sequence conservation (left panel; with plum being the most conserved and cyan the most variable) and upper right insets show electrostatic (**[D]** and **[E]**; blue is electropositive, red electronegative) or

Table 2. Data Collection, Model Refinement, and Final Structure Statistics for ClpT1 and ClpT2

	ClpT1	ClpT2
Crystallographic data collection statistics		
Space group	$P2_12_12_1$	C2
Cell dimensions:		
a = (Å)	30.4	104.15
b = (Å)	109.2	57.77
c = (Å)	120.5	61.65
b = (°)	90	98.17
Wavelength (Å)	0.979098	1.54158
Resolution (Å)	2.4	2
Unique observations	16,579	23,802
Completeness (last shell)[a]	0.998 (1.00)	0.954 (0.678)
Redundancy (last shell)[a]	7.9 (8.1)	4.9 (2.6)
$<I/\Sigma(I)>$ (last shell)[a]	12.7 (2.1)	21.6 (3.5)
R_{sym} (last shell)[a]	0.089 (0.99)	0.066 (0.457)
X-ray structure refinement statistics		
R_{cryst}	0.206	0.173
R_{free}[b]	0.253	0.207
Asymmetric unit contents		
Water molecules	24	288
Other molecules	2 Cl^-	2 SO_4, 1 Cl^-
Average ADPs ($Å^2$)		
Protein	75.3	28.4
Water	51.9	31.1
r.m.s.d. bond lengths (Å)	0.011	0.0085
r.m.s.d. bond angles (°)	1.461	1.134
Ramachandran favored (%)	95.2	96.1
Ramachandran outliers (%)	0.4	0.3

[a]The last shell includes all reflections between 2.46 and 2.40 Å for ClpT1 and between 2.1 and 2.0 Å for ClpT2.
[b]R_{free} calculated using 5% of the data that were chosen randomly.

residues to form a binding pocket that specifically recognizes surface-exposed glutamic acid residues, while surrounding motifs extend the interaction surface to recognize other features of the cognate ligand, most often an α-helix (Erbse et al., 2008; Kirstein et al., 2009; Kress et al., 2009; Striebel et al., 2009). In the *B. subtilus* ClpC N-domain, Thr-31 and Thr-81 in this glutamate binding pocket binds Glu-184 of adaptor MecA (Wang et al., 2011) (Supplemental Figure 6D). Similarly, in *E. coli* ClpA, Glu-28, Thr-81, and the backbone amines at the N-terminal end of αB recognize Glu-79 of ClpS (Guo et al., 2002; Zeth et al., 2002) (Supplemental Figure 6E). The equivalent residues in ClpT2 (Thr-119 and Glu-120) (Figure 4D, lower panel) at the N-terminal end of αB along with Thr-172 are conserved in ClpT2 (and also ClpT1), suggesting a conserved role in recognizing glutamate. In ClpT1, this pocket binds Glu-159 of the adjacent ClpT1 molecule in each asymmetric unit within the crystal (Supplemental Figure 6C). This region of the protein contains some additional conserved residues (e.g., Lys-154, Lys-158, and Asp-160) and is flanked in the structure by the conserved hydrophobic MYFF motif (Figures 4A and 4B; next section) in the αD- αE loop (see sequence logo in Supplemental Figure 2). To test the in vivo significance of the predicted glutamate binding pocket in ClpT1 and ClpT2, we transformed the *clpt1-2 clpt2-1* double mutant with StrepII-tagged variants of ClpT1 (T111V and

Figure 4. (continued).

hydrophobicity (**[F]**; orange is hydrophobic and green hydrophilic, Eisenberg scale) with the location of the detailed view (lower panels) marked with a dashed box.

(D) The glutamate binding surface of ClpT2. This figure is oriented very similar as **(A)** to **(C)**. The glutamate binding pocket in ClpT2 is comprised of Thr-119 and Glu-120 at the N-terminal end of αB, along with Thr-172; glutamate has been observed to mediate biologically relevant interactions with the homologous pocket in the N-domains of ClpA (with ClpS) and ClpC (with MecA) (Supplemental Figures 6B, 6D, and 6E). In ClpT1, the equivalent residues bind a glutamate from a neighboring molecule, showing that the essential recognition elements remain intact (Supplemental Figure 6C).

(E) Candidate basic binding pocket on the face of ClpT2. This face has a large number of conserved hydrophobic (e.g., Met-104, Leu-107, and Ile-128) and basic (e.g., Lys-100, Arg-110, Lys-111, Lys-113, and Arg-149) residues and is flanked by the hydrophobic MYFF motif. This pocket in *E. coli* ClpA N-domain mediates interactions between the N-domain and the rest of the chaperone structure (Supplemental Figure 5G).

(F) The hydrophobic binding pocket formed between αA and αE; view is down the quasi 2-fold axis. The equivalent surface is similarly hydrophobic and is used to bind substrates in *B. subtilis* ClpC and *V. cholera* ClpV (Supplemental Figures 6H and 6I).

T164V) and ClpT2 (T119V and T172V). Surprisingly, all four ClpT1 or ClpT2 mutant constructs fully complemented the double mutant (Supplemental Figure 7). This indicates that despite the conservation of these residues, this pocket is not required for essential ClpT functions and perhaps that ClpT does not bind adaptors, such as ClpS1, or as yet unidentified ones. However, it cannot be totally excluded that the relatively conservative Thr→Val (similar sized uncharged polar → apolar) mutations retain sufficient interaction strength to suppress the growth phenotype seen in the mutants.

Due to the internal rotational symmetry of Clp N-domains, the arrangement of helices in the glutamate binding pocket centered on αB is repeated on the opposite side of the molecule, centered on the N-terminal end of αF. In *B. subtilis* ClpC, this pocket also has the appropriate T/E/T motif and is used to bind Glu-189 of MecA (Wang et al., 2011). In ClpT, the T/E/T motif is absent and the packing of nearby loops narrows the pocket, implying that this pocket is unlikely to mediate any analogous interactions; this is consistent with our previous (Nishimura et al., 2013) and current observations that ClpT proteins do not interact with adaptor proteins.

A third interaction surface in chaperone N-domains and ClpT1 and ClpT2 is found on the reverse face of the glutamate binding pocket, and this surface is characterized by a band of basic residues flanked on either side by conserved hydrophobic residues (Figure 4E, upper panel). The top hydrophobic band is formed by the MYFF motif, while the lower hydrophobic band is formed by residues including Met-104, Leu-107, and Ile-128. Among the conserved basic residues are Arg-110, Lys-111, Lys-113, Arg-149, and Lys-158, while Glu-108 and Glu-167 are acidic residues interspersed among the basic residues (Figure 4E, lower panel). In *E. coli* ClpA, this surface is used by the N-domain to bind to the AAA domain. The strong conservation of this pocket in ClpT implies that it may also have an important function in ClpT.

The fourth potential binding pocket in ClpT2 is a large exposed hydrophobic patch located between the long helices αA and αE (Figure 4F). Trp-94, Ile-99, Phe-102, Leu-171, Leu-179, and Leu-183 are all conserved as hydrophobic residues, while some adjacent hydrophilic residues including Gln-176 and Asp-180 are also absolutely conserved in ClpT2 (and very conserved in ClpT1). The equivalent surface, similarly hydrophobic, is used by the N-domain of the AAA protease *V. cholera* ClpV to recognize its substrate VipB in type VI protein secretion (Pietrosiuk et al., 2011). In ClpA, this region interacts with ClpS and is also implicated in peptide binding (Xia et al., 2004), while in *Mycobacterium* ClpC, this region is the target of the antimicrobial cyclomarin A, implying a possible role in substrate interaction (Vasudevan et al., 2013) (Supplemental Figures 6H and 6I). Unless required for function, proteins generally avoid exposing extensive hydrophobic patches as they are prone to aggregation; the presence of this patch here implies a likely role in protein-protein interaction, albeit with an unknown partner.

The MYFF Motif Is Functionally Important

The long αD-αE loop contains a hydrophobic, aromatic-rich sequence motif, MYFF, in Arabidopsis ClpT1 and ClpT2 and generally conserved as (M/L)(Y/F)(F/Y/W)F in both ClpT1 and ClpT2 (Supplemental Figure 2). In our structures, this motif is not part of the hydrophobic core of the protein, but instead is ordered by packing interactions in chain A of ClpT2, partially ordered in both ClpT1 monomers and disordered in ClpT2 chain B. This very hydrophobic motif is therefore exposed on the protein surface in the middle of a flexible loop, with a strong tendency toward disorder. Its lack of interaction with the core ClpT structure, along with the position of this motif at the periphery of two candidate binding surfaces (the glutamate binding and basic sites) suggests that this motif may be involved in an external interaction.

To test the in vivo significance of the MYFF motif of ClpT1 or ClpT2, we transformed the *clpt1-2 clpt2-1* or *clpt1-2 clpt2-2* double mutant with variants of ClpT1 and ClpT2 (MYFF→AAAA). Unlike *clpt1 clpt2 CLPT1* or *clpt1 clpt2 CLPT2* lines, which showed full complementation, *clpt1 clpt2 CLPT1*(MYFF→AAAA) or *clpt1 clpt2 CLPT2*(MYFF→AAAA) did not exhibit a wild-type-like phenotype (Figure 5A; see Supplemental Figure 8 for older plants). They showed the same small, yellow, pale-green phenotype like *clpt1-2 clpt2-2*, implying that they could not complement the double homozygous mutant. The overexpression of the variant ClpTs form was confirmed by immunoblotting against ClpT antisera (Figure 5B). The lack of complementation of the mutant phenotype shows that the MYFF motif of ClpT is crucial for Clp protease and chloroplast function and plant development. We then tested the ClpPR core assembly state and if the variant ClpT1 and ClpT2 proteins could interact with the ClpPR core complex or ClpP ring. To that end, chloroplast stromal proteins were extracted under nondenaturing conditions and proteins were separated by 1D-BN-PAGE, followed by immunoblotting with ClpR2 and ClpT1 serum (Figure 5C). The *clpt1-2 clpt2-2 CLPT1*(MYFF→AAAA) mutants failed to stabilize the ClpPR core and showed about the same level of Clp core assembly as the *clpt1-2 clpt2-2* double mutant. In contrast, expression of the StrepII-tagged wild-type-like ClpT1 did restore the ClpPR assembly state determined by blue native PAGE (BN-PAGE; Figure 5C). Using BN-PAGE and two-dimensional PAGE, we showed that variant ClpT could only interact with the individual ClpP ring and not with the 350-kD core (Figures 5C and 5D). These data demonstrate that the MYFF motif is required for stabilization of ClpP and ClpR ring interactions, but not strictly for interaction to the ClpP ring. These data also show that ClpT1 and ClpT2 binding to the ClpP ring is not enough for core stabilization, and we suggest that binding of this extended hydrophobic MYFF motif to the P-ring results in an allosteric change in the P-ring, leading to stabilization of the overall complex.

DISCUSSION

ClpT Proteins Are Unique to Higher Plants

Sequence analysis strongly suggests that ClpT proteins are derived from ClpC chaperones but that these ClpT proteins are absent in cyanobacteria; this is significant because the function of ClpT concerns ClpPR protease activity and these chloroplast progenitors also have ClpR proteins and a mixed ClpP3R

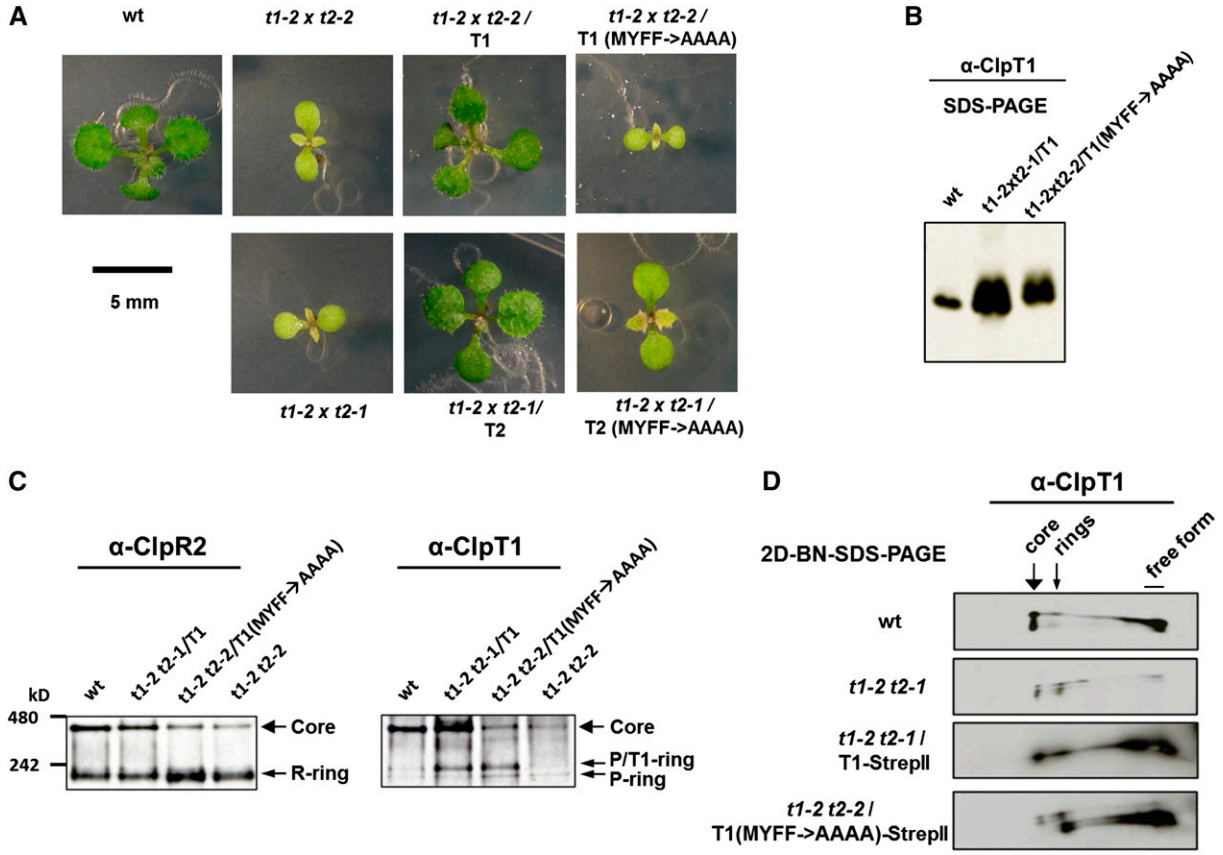

Figure 5. Complementation of *clpt1 clpt2* with 35S-Driven cDNAs for *CLPT1*, *CLPT1*(MYFF→AAAA), *CLPT2*, and *CLPT2*(MYFF→AAAA) and Assembly State of the ClpPRT Proteins.

(A) Comparison of the wild type, *clpt1-2 clpt2-1*, *clpt1-2 clp2-2*, and *clpt1-2 clpt2-2* transformed with 35S-driven cDNA for *CLPT1* or *CLPT1*(*MYFF->AAAA*), and *clpt1-2 clp2-1* transformed with 35S-driven *CLPT2* or *CLPT2*(MYFF→AAAA). Plants were grown for 11 d on half-strength Murashige and Skoog agar plates + 2% sucrose under continuous light at 100 μmol photons m^{-2} s^{-1}. Older, more developed plants grown further after transfer to soil are shown in Supplemental Figure 8 and further illustrate the lack of phenotypic complementation for the MYFF constructs. Bar = 5 mm.

(B) Accumulation levels of ClpT1 protein in *clpt1-2 clpt2-1 CLPT1* and *clpt1-2 clpt2-2 CLPT1*(MYFF→AAAA) compared with the wild type. Total soluble leaf proteins were extracted from each line. After SDS-PAGE, proteins were transferred to blots and probed with ClpT1 antiserum. Ten micrograms was loaded in each lane.

(C) Assembly state of the ClpPRT proteins determined by immunoblot analysis after native gel electrophoresis. Stromal proteins obtained from isolated chloroplasts from the wild type (wt), *clpt1-2 clpt2-2*, *clpt1-2 clpt2-1/T1*, and *clpt1-2 clpt2-2 CLPT1*(MYFF→AAAA) were separated on native gels, transferred to blots, and probed with antisera against ClpR2 and ClpT1. The larger arrows indicate ClpPRT core complexes (350 to 400 kD), while the smaller arrows indicate ClpP/T1-ring, P-ring, or R-ring. Thirty micrograms of stromal protein was loaded in each lane.

(D) Immunoblot analysis after 2D electrophoresis. Protein complexes from the wild type, *clpt1-2 clpt2-1* double mutant, *clpt1-2 clpt2-1 CLPT1*-StrepII, and *clpt1-2 clpt2-2* CLPT1(MYFF→AAAA)-StrepII were separated as in **(C)** by BN-PAGE (first dimension) followed by SDS-PAGE (second dimension). The 2D gel was electroblotted and probed with antisera against ClpT1. The positions of detected ClpPRT core, ring, and free form are indicated.

complex. However, the organization of this cyanobacterial complex is different in that the two heptameric rings in the ClpP3R complex are symmetrical (Stanne et al., 2007), while the ClpP and ClpR rings in chloroplasts are asymmetrical with each having their own set of proteins (reviewed in Nishimura and van Wijk, 2014). Moreover, the ClpC chaperones in higher plant chloroplasts likely only interact with the R-ring (based on sequence comparison of key residues in cyanobacteria ClpP3 and ClpR), whereas ClpT proteins directly bind to the P-ring (Nishimura and van Wijk, 2014). This suggests that higher plant ClpT proteins have specifically coevolved with the ClpPR proteins to ensure a fully functional ClpPR complex, by facilitating the formation/stabilization/activation of the ClpPR complex. An alternative hypothesis for the presence of ClpT proteins is that they facilitate the proteolysis of a specific set of proteins, e.g., by binding to specific intrachloroplast membranes, binding to chloroplast-specific adaptors, or binding to specific protease substrates. The biochemical, structural, and proteomics analysis in this study strongly suggests that ClpT evolved to ensure a functional ClpPR complex, rather than facilitating degradation of specific proteins. Finally, monocots only have ClpT1 proteins and also a few dicots have either only ClpT1 or ClpT2, suggesting that ClpT1 and ClpT2 proteins have largely redundant functions.

Double Homozygous *CLPT* Mutants Are Viable but Show a Clear Growth and Developmental Phenotype

Based on the screening of 100 progeny, it was previously reported that double homozygous mutants (*clpt1-1 clpt2-1*) are not viable (Sjögren and Clarke, 2011). However, when we crossed and then selfed each *CLPT1* and *CLPT2* allele, we produced double homozygous mutants that survived well on soil, flowered, and generated viable seeds. Since the two *CLPT* genes are located on the same chromosome (*CLPT1*, At4g25370; *CLPT2*, At4g12060; physical distance between *CLPT1* and *CLPT2* is ~5.7Mb), we screened hundreds of seedlings to identify the double homozygous mutants. For example, in the case of *clpt1-1 clpt2-1*, we identified 15 double homozygous mutants out of 1151 seedlings. Considering a genetic distance of 1% recombination corresponds, on average, to a physical distance of ~250 kb in Arabidopsis (Lukowitz et al., 2000), the chance of recombination between *CLPT1* and *CLPT2* is ~23%. Thus, the probability of double homozygous (*aabb*) mutant based on 23% recombination is 0.013. This matches well with our finding of 15 double homozygous mutants out of 1151 seedlings. This explains why the previous report failed to identify double homozygous mutants. Importantly, the viable double mutants allowed us to analyze the role of ClpT1 and ClpT2 in ClpPR stability and proteostasis and to determine (1) if ClpT1 and ClpT2 can interact independently with the ClpPR core (as opposed to an interdependent interaction), (2) if ClpT1 and ClpT2 have redundant functions, and (3) the molecular consequences for the lack of ClpT1 and ClpT2 on leaf development and chloroplast biogenesis, function, and proteostasis.

Side-by-side comparison of the *clpt1-2 clpt2-1* double mutant to the *CLPR2* knockdown line *clpr2-1* (with ~20% of ClpR2 levels) showed that the *clpt* double mutant was somewhat smaller in stature, with quite similar patterns of leaf virescence and serration, independent of leaf development and light regime. However, whereas null mutants for the genes encoding ClpR2, ClpP3, and ClpR4 are seedling lethal and null mutants for the genes encoding ClpP4 and ClpP5 are embryo lethal, the double mutant in *CLPT1* and *CLPT2* does not require sucrose and is viable on soil. This demonstrates that ClpT1 and ClpT2 are not strictly required for Clp protease function and indicates that in their absence ClpPR capacity is reduced to ~20%. However, unlike both *clpt2* alleles, the strongest *clpt1* mutant (*clpt1-2*) did accumulate a ClpT1 cross-reacting band, albeit at higher molecular mass. Whereas we could not detect ClpT1 in this *clpt1-2* allele by MS/MS analysis, *clpt1-2* may not be a strict null mutant; it is thus possible that complete loss of ClpT1, together with complete loss of ClpT2, does lead to seedling (or embryo) lethality.

The Proteome Phenotype Suggests Limited Clp Protease Capacity

Comparison of the proteome phenotype of the *clpt1-2 clpt2-1* double mutant versus loss-of-function mutants of *CLPR2*, *CLPR4*, and *CLPP3* (reviewed in Nishimura and van Wijk, 2014) showed very similar patterns of under- and overaccumulation of proteins. For instance, the unfoldase ClpB3, maturase HSP90, the CPN60 chaperones, as well as the three chloroplast elongation factors were all significantly upregulated. The strong upregulation of plastoglobular proteins indicated significant stress levels similar as observed in the other Clp mutants. We did not observe proteins that were specifically over- or underaccumulating in the ClpT mutant but not in the ClpPR core mutants. Hence, the ClpT mutant proteome phenotype is easiest explained by a strongly reduced ClpPR protease capacity. However, clearly, the ClpT double mutant must have significant Clp protease activity because complete loss of ClpPR capacity leads to embryo or seedling lethality. We thus conclude that ClpT proteins do not appear to facilitate the proteolysis of a specific class of proteins, unlike, for example, the adaptor NblA for degradation of phycobilisomes in cyanobacteria (Karradt et al., 2008; Baier et al., 2014) but rather facilitate ClpPR activity, as discussed further below.

The Double Mutant Phenotype Cannot Be Explained by Loss of ClpPR Core Assembly

In a recent study (Sjögren and Clarke, 2011), it was proposed that individual ClpP and ClpR rings exists in the stroma and that ClpPR activity is regulated through (reversible) association of ClpP and ClpR rings by sequential activity of ClpT1 and ClpT2. This model was essentially based on results from BN-PAGE analysis of wild-type proteins showing that <50% of ClpPR rings are assembled in a ClpPR core complex, but rather exist as individual rings. The percentage of assembly ClpPR core was even lower in the weak *clpt1-1* (~30%) and the *clpt2-1* null mutants (~10%). Upon addition of recombinant ClpT1 and ClpT2, the percentage of observed ClpPR cores increased. Their model was further inspired by the erroneous observation that no double mutants for ClpT1 and ClpT2 could be obtained, even when using the weak *clpt1-1* allele, as we discussed above. This study, combined with our previous studies (reviewed in Nishimura and van Wijk, 2014), contradicts this model based on the following observations: (1) in-house colorless native PAGE (CN-PAGE), gel staining, and MS analysis (Peltier et al., 2004, 2006), as well as immunoblotting of CN-PAGE gels with anti-polyHis serum of the *clpr2-1* mutant complemented with polyHIS$_6$-tagged ClpR2 (Rudella et al., 2006), indicated that in wild-type chloroplasts, a single ClpPR complex accumulates without detectable individual free ClpP and ClpR rings; and (2) the ClpT double mutant *clpt1-2 clpt2-1* shows a strong growth phenotype, yet the observed level of ClpPR core accumulation is at least as high as the *clpt1-2* single mutant, which lacks a growth phenotype.

ClpT1 and ClpT2 Structure, Modeling, and Experimental Testing the Interactions between ClpT and the Clp Protease Core

The high-resolution structures of ClpT1 and ClpT2 clearly demonstrated the similarity to N-domains of Clp chaperones. These structures allowed us to suggest, and subsequently experimentally test, possible interaction domains and motifs between ClpT1, ClpT2, and the ClpPR core. Out of the three most obvious interaction surfaces, we showed that the MYFF motif is

essential for ClpT function. The hydrophobic nature of this motif is reminiscent of the hydrophobic IG(F/L) motif used by *E. coli* ClpA/X (conserved in Arabidopsis ClpC1, ClpC2, and ClpD; Peltier et al., 2004) to bind to hydrophobic grooves in the adaxial side of the ClpP ring (Kim et al., 2001). This motif in ClpT may be more hydrophobic as only one such motif will be utilized for interaction, versus the six interactions used to recruit ClpA/C hexamers (one interaction contact for each ClpA/C) (Kim et al., 2001); the more extended hydrophobic region in ClpT may in turn require a longer hydrophobic binding groove on the ClpP ring. Thus, the structure suggests that MYFF motif of ClpT might be a key motif for interacting with the ClpPR core. The MYFF motif is likely to act in synergy with either the glutamate binding pocket (though the nonessentiality of the Thr-119 and Thr-172 possibly argues against this) or the basic pocket located on the opposite face. This involvement of a larger binding pocket could explain why ClpT is able to interact with the ClpP ring. The MYFF motif might then stabilize the 350-kD core through two possible modes of action, as discussed in the next section.

ClpT1 and ClpT2 Affect ClpPR Protease Capacity

The observed loss of ClpPR core assembly on native gels likely reflects the weakened interactions in absence of (or at low levels) of ClpT proteins. Depending on the forces during native gel electrophoresis (different protocols), different levels of intact ClpPR core are observed. Based on all available information, we suggest two possible mechanisms for the stabilization and activation of ClpPR protease by ClpT (Figure 6). In the most attractive model (Figure 6A), ClpT binds to the ClpP ring and inserts the MYFF loop into a hydrophobic pocket. This interaction then allosterically stabilizes the ClpP-ClpR ring interaction. Inter-ring allostery is a well-established phenomenon in ClpP; for example, in the bacterial ClpAP system, ClpA binding to one ClpP ring also activates the protease activity of the distal ClpP ring through in large conformational changes (Maglica et al., 2009; Liu et al., 2014). Furthermore, various small molecules (e.g., ADEPs) have recently been identified that activate the ClpP complex by conformational changes to the ring structure visualized by cryoEM and single particle averaging (Alexopoulos et al., 2012; Liu et al., 2014). In the second, less favored model (Figure 6B), ClpT binds primarily to the ClpP ring, while the MYFF loop binds a hydrophobic pocket on the ClpR ring, directly stabilizing the ClpP-ClpR interaction. We thus propose that ClpT1 and ClpT2 stabilize the ClpP and ClpR ring interactions and likely activate the ClpPR complex through allosteric effects (structural conformations).

Interactions between ClpT1, ClpT2, and Adaptors and Accumulation of Free ClpT Proteins

Both the primary sequences and structures of ClpT1 and ClpT2 demonstrate high similarity with the N-domains of bacterial (and plant) ClpA/C chaperones. The main function of this N-domain is binding of adaptor proteins (e.g., ClpS and MecA) and substrates (see Introduction and Sauer and Baker [2011]). Based on

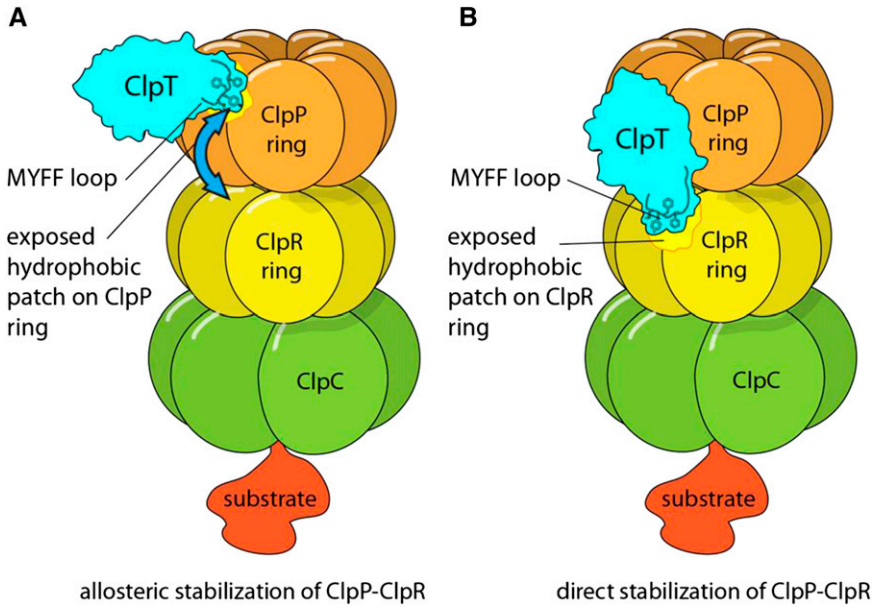

Figure 6. Models for the Role of ClpT1 and ClpT2 in the Clp Protease System in Plastids.

It is conceivable that the outer adaxial surface of the R-ring could be affected indirectly by ClpT binding through the structural dynamics of the core complex, thus influencing ClpC affinity and/or access to the ClpPR pore.

(A) ClpT binds to the ClpP ring and inserts the MYFF loop into a hydrophobic pocket. This interaction then allosterically stabilizes the ClpP-ClpR ring interaction.

(B) ClpT binds primarily to the ClpP ring, while the MYFF loop binds a hydrophobic pocket on the ClpR ring, directly stabilizing the ClpP-ClpR interaction.

this homology, we previously speculated that ClpT1 and ClpT2 could interact with chloroplast ClpS1 (or other unknown adaptors) and perhaps substrates (Peltier et al., 2004). However, StrepII affinity purifications, coimmunoprecipitation with the specific anti-ClpT1 and ClpT2 anti-sera, or previous interaction analysis with recombinant ClpS1 and ClpT (Nishimura et al., 2013) did not detect such interactions. Nevertheless, one can still not entirely exclude that such functional interactions might exist, since perhaps ClpS1-ClpT interactions may only occur when ClpS1 interacts with specific substrates. Chloroplast ClpT proteins were initially identified as members of the ClpPR based on native page (CN-PAGE, BN-PAGE, and native isoelectric focusing) followed by staining and mass spectrometry (Peltier et al., 2001, 2004) with on average one ClpT1 and one ClpT2 per complex as estimated by silver and Coomassie blue staining and theoretical correction for amino acid composition (Peltier et al., 2004). The in vivo StrepII tagging and affinity experiments showed that ClpT1 and ClpT2 independently bind to the ClpPR core complex. Current and previous label-free spectral counting analysis of stroma and total leaf extracts suggests approximately four to five ClpT proteins per ClpPR core complex. With two ClpT proteins bound to each ClpPR complex, this would suggest that 50% of ClpT proteins are unbound. Recent estimates by Sjögren and Clarke (2011) suggest that only 5% of ClpT is bound to the ClpPR core; however, given the relatively weak and salt sensitive interactions between ClpT and the ClpPR core and the relatively harsh nature of BN-PAGE (depending on the procedure used), this strongly underestimates the fraction of bound ClpT. Nevertheless, the significance of free stromal ClpT proteins remains to be determined. The suggestion that recombinant ClpT interacts with ClpC2 and ClpD chaperones and stimulates ATP hydrolysis activity by ClpD (Colombo et al., 2014) also warrants further investigation.

Interactions between ClpT and CPN20

The in vivo ClpT StrepII tagging and affinity experiments also identified a CPN20 as a candidate interacting protein with ClpT1 and ClpT2, most likely when these ClpT proteins do not interact with the ClpPR core. CPN20 is part of the family of Type I chaperonins that function in protein folding together with CPN60 proteins and CPN10 proteins (Koumoto et al., 1999; Sharkia et al., 2003; Vitlin Gruber et al., 2013). It remains to be determined if and how CPN20 has a functional relationship to ClpT1 and ClpT2.

Future Directions

The structures of ClpT1 and ClpT2 allowed us to assess their possible interaction domains and surfaces with the ClpPR core. However, better understanding of the docking and functional interaction of ClpT to the ClpP ring, and perhaps the ClpR ring, is necessary to determine how ClpT influences ClpPR stabilization and activity. This will require a better understanding of the organization of the ClpP/R rings, in particular the order of the ClpP and ClpR subunits within each ring, as well as experimental determination of direct ClpPR binding partners for ClpT1 and ClpT2. The availability of Arabidopsis StrepII-tagged ClpP3, ClpR4, ClpT1, and ClpT2 lines in their respective null backgrounds should allow such interaction mapping by affinity purification, cross-linking, and mass spectrometry. Based on such information, better homology models for the P-ring and R-ring can then be created, thus allowing more efficient testing of docking models for ClpT1 and ClpT2. This could explain molecular mechanisms involving the conserved ClpT proteins in higher plants.

METHODS

Plant Growth, Mutant Isolation, and RT-PCR Analysis

T-DNA insertion lines in Columbia-0 for *CLPT1* (AT4G25370) and *CLPT2* (AT4g12060) are SALK_052772 (*clpt1-1*), GK-285A05 (*clpt1-2*), SAIL_340A10 (*clpt2-1*), and SALK_132943 (*clpt2-2*). The location of the T-DNA insertions was confirmed by DNA sequencing. Genotyping and RNA extraction were performed as described previously (Rudella et al., 2006). Various growth conditions are detailed in the figure legends. For RT-PCR, total RNA was isolated with an RNeasy plant mini kit (Qiagen). The first strand was synthesized from equal amounts of total RNA with Superscript III reverse transcriptase (Invitrogen). We tested 15, 20, 25, and 30 cycles for the primer pairs. Fifteen cycles were insufficient to visualize all transcripts, while 20 and 25 cycles best allowed us to visualize the transcripts, and we observed good linearity for 20 and 25 cycles. Primers for genomic PCR and RT-PCR analysis and various complementations are listed in Supplemental Table 2. Transcripts were quantified using ImageJ (http://imagej.nih.gov/ij/).

Complementation

Full-length and various mutagenized forms of *CLPT1* and *CLPT2* cDNA fragments were PCR amplified, and the C-terminal StrepII sequence was attached using Taq polymerase. Primers for complementation are also listed in Supplemental Table 2. The PCR products were subcloned into pCR8/GW/TOPO vector (Invitrogen). Using LR clonase, the DNA was introduced into pEARLEYGATE100 Gateway destination plant binary vector (Curtis and Grossniklaus, 2003). Competent cells of *Agrobacterium tumefaciens* strain GV3101 were transformed with the binary vector. The *clpt1 clpt2* double homozygous plants were used for Agrobacterium-mediated plant transformation by the floral dipping method. Transformants were screened using 10 mg/mL DL-phosphinothricin (Crescent Chemical). Complemented plants were selected and verified by PCR genotyping.

Phylogenetic Analysis

Protein sequences were collected from Phytozome v9 (http://www.phytozome.net/). Fifty ClpT proteins from moss and 31 angiosperms were aligned using Muscle (http://toolkit.tuebingen.mpg.de/muscle) with 30 times of iterations and ClustalW output format. The aligned sequences were edited to remove their predicted chloroplast transit peptide portions, gaps, insertions, and extensions with Jalview (http://www.jalview.org/) and then converted to the PHYLIP format. A phylogenetic tree was generated using the RAxML HPC BlackBox interface with the general time reversal model of the protein substitution matrix on the CIPRES Science Gateway (http://www.phylo.org/index.php/portal/). The resulting phylogenetic tree was visualized by FigTree (http://tree.bio.ed.ac.uk/software/figtree/), and significant RAxML bootstrap values (>50) were shown at the nodes of the tree. Original protein sequences and multiple sequence alignment are available as Supplemental Data Sets 1 and 2.

Chloroplast Stroma and Total Leaf Proteome Isolation for Analysis of Clp Assembly States

For chloroplast stroma isolations, leaves of the wild-type and various mutant alleles were briefly homogenized in grinding medium (50 mM HEPES-KOH, pH 8.0, 330 mm sorbitol, 2 mM EDTA, 5 mM ascorbic acid, 5 mM cysteine, and 0.03% BSA) and filtered through a nylon mesh. The crude plastids were then collected by a 2-min spin at 1100*g* and further purified on 35 to 85% Percoll cushions (Percoll in 0.6% Ficoll and 1.8% polyethylene glycol) by a 10-min spin at 3750*g* and one additional wash in the grinding medium without ascorbic acid, cysteine, and BSA. Chloroplasts were subsequently lysed in 10 mM HEPES-KOH, pH 8.0, 5 mM $MgCl_2$, and 15% glycerol with a mixture of protease inhibitors under mild mechanical disruption. The lysate was then subjected to ultracentrifugation (100,000*g*) to pellet the membrane components. The supernatant (stroma) was then collected. Protein amounts were determined using the BCA protein assay kit (Thermo Scientific). For total leaf proteome isolation under nondenaturing conditions, total leaf material was ground in liquid nitrogen and solubilized in 50 mM HEPES-KOH, pH 8.0, 15% glycerol, and 10 mM $MgCl_2$ with protease inhibitor cocktail. The suspension was then filtered through Miracloth and spun at 100,000*g*.

Affinity Purification of StrepII-Tagged ClpT1 and ClpT2

Isolated stromal protein (2 mg) from the *clpt1-2 clpt2-1* double mutant (negative control) and transgenic StrepII-tagged plants was loaded on a Strep-Tactin superflow high capacity column (IBA). Glycerol (15%) was included in all the buffers to preserve the Clp core complex. After washing with 1 mL of washing buffer (50 mM HEPES-KOH, pH 8.0, 10 mM $MgCl_2$, 75 mM NaCl, and 15% glycerol) five times, elution was performed with 0.5 mL Buffer E (washing buffer with 2.5 mM Desthiobiotin) six times.

Native PAGE and BN-SDS-PAGE (2D) Analysis

Light-blue native PAGE was performed for separation of stromal and total leaf extracts under nondenaturing conditions using the NativePAGE Novex gel system (Invitrogen) with precast 4 to 16% acrylamide Bis-Tris gels (Invitrogen). For 2D electrophoresis, the lanes on the blue native PAGE gel were cut out and incubated in SDS-PAGE equilibration buffer (6 M urea, 2% SDS, 50 mM Tris-HCl, pH 6.8, 30% glycerol, and 5 mM DTT) at room temperature for 1 h. The gel was loaded on top of the gel and was separated by SDS-PAGE.

Immunoblot Analysis

For immunoblots, proteins were blotted onto nitrocellulose or polyvinylidene fluoride membranes and probed with antibodies using chemiluminescence for detection, following standard procedures. Antisera against ClpP6, ClpT1, and ClpT2 were generated in rabbits against protein domains [ClpP6 (Δ1-51), ClpT1 (Δ1-64), and ClpT2 (Δ1-75)] overexpressed in *Escherichia coli*. Crude antisera were affinity purified using these overexpressed antigens as bait. StrepII polyclonal antibody was purchased from GenScript.

Cloning, Overexpression, and Purification of Mature ClpT1 and ClpT2 in *E. coli*

The cDNAs encoding ClpT1 and ClpT2 were cloned out of *Arabidopsis thaliana* cDNA. The fragments encoding mature ClpT1 (ClpT1 Δ1-64) and mature ClpT2 (ClpT2 Δ1-75) were cloned into the expression vector pET-28b (Novagen). The plasmids pET28-ClpT1 Δ1-64 and pET28-ClpT2 Δ1-75 were transformed into BL21 (DE3) *E. coli* cells. Overnight small-scale cultures were inoculated into Luria-Bertani media containing kanamycin (50 μg/mL), grown at 3°C until OD_{600} reached 0.6, and then induced with isopropyl β-D-1-thiogalactopyranoside (1 mM final concentration) at 37°C for 3.5 h. Cells were harvested by centrifugation and resuspended in lysis buffer (10 mM imidazole, 50 mM NaH_2PO_4, pH 8.0, and 300 mM NaCl). After sonicating on ice for six 10-s bursts, the lysate was centrifuged at 10,000*g* for 20 min at 4°C. The cleared lysate was then mixed with the Ni-NTA His Bind slurry by shaking at 4°C for 2 h. The lysate-Ni-NTA His Bind mixture was loaded into a column and then the column was washed with wash buffer (20 mM imidazole, 50 mM NaH_2PO_4, pH 8.0, and 300 mM NaCl) three times and then finally eluted with a step gradient (40 to 250 mM imidazole with 30 mM increments, 50 mM NaH_2PO_4, pH 8.0, and 300 mM NaCl). The protein eluted maximum at 130 and 160 mM imidazole concentration.

Structure Determination

ClpT1 was crystallized from 10% polyethylene glycol 6000 and 0.2 M tripotassium citrate; ClpT2 was crystallized from 1.6 M ammonium sulfate, 10% dioxane, and 0.1 M MES, pH 6.5. Crystals were frozen in the cryostream after the surface water was removed by paratone N-oil. ClpT2 data were collected on a Rigaku rotating anode (45 kV, 30 mA) with a Rigaku 4k CCD detector; data were processed using the Proteum package and scaled using XPREP. ClpT1 data were collected at the Canadian Synchrotron Light Source (beam line CMCB) and processed in XDS (Kabsch, 2010). The structure of ClpT2 was determined by molecular replacement with Phaser (McCoy et al., 2007), using the structure 3FH2 (*Corynebacterium glutamicum*) as a search model. ClpT1 was then determined using the ClpT2 structure as a search model. Both structures were rebuilt in Coot (Emsley and Cowtan, 2004) and refined in Phenix (Adams et al., 2002), using TLS parameters. The ClpT1 refinement included torsion angle NCS restraints. Residues 76 to 81 of ClpT2 show some weak electron density in chain A, but the nonconserved nature of this region and their disorder in chain B argue that the partial order of this region may be an artifact of the crystallization process. The structures and x-ray diffraction data sets of ClpT1 and ClpT2 have been deposited to the Protein Data Bank (www.rcsb.org) with reference codes 4Y0B and 4Y0C, respectively.

Proteomics and Mass Spectrometry

Three biological replicates per genotype were analyzed resulting in 66 MS/MS runs. Homozygous *clpt1-2 clpt2-1* plants were grown under a short-day cycle (10 h/14 h of light/dark at 100 μmol photons m^{-2} s^{-1}) for 41 d. Total leaf proteins were extracted under denaturing conditions after grinding 250 to 350 mg fresh leaves in liquid N_2 into a fine powder, followed by removal of cell debris on Fritt spin columns (pore size 30 μm) as described (Friso et al., 2011). This was performed in three biological replicates. Protein concentrations were determined using the BCA Protein Assay Kit (ThermoFisher). Fifty micrograms of total leaf protein of *clpt1-2 clpt2-1* and wild-type samples were each run out on a Bio-Rad Criterion Tris-HCl precast gels (10.5 to 14% acrylamide gradient) using the three biological replicates. Each of the six gel lanes were cut into 11 bands followed by reduction, alkylation, and in-gel digestion with trypsin as described (Shevchenko et al., 2006; Friso et al., 2011).

The resuspended peptide extracts were analyzed by data-dependent MS/MS using an on-line LC-LTQ-Orbitrap (Thermo Electron). Peptide samples were automatically loaded on a guard column (LC Packings MGU-30-C18PM) via an autosampler followed by separation on a PepMap C_{18} reverse-phase nanocolumn (LC Packings nan75-15-03-C18PM) using 90-min gradients with 95% water, 5% acetonitrile, and 0.1% formic acid (solvent A), and 95% acetonitrile, 5% water, and 0.1% formic acid (solvent B) at a flow rate of 200 nL/min. Two blanks were run after every sample (see Zybailov et al. [2009] for the gradient and sample injection scheme). The acquisition cycle consisted of a survey MS scan in the Orbitrap with a set mass range from 350 to 1800 *m/z* at the highest

resolving power (100,000) followed by five data-dependent MS/MS scans acquired in the LTQ. Dynamic exclusion was used with the following parameters: exclusion size, 500; repeat count, 2; repeat duration, 30 s; exclusion time, 180 s; exclusion window, ±6 ppm or ±100 ppm. Target values were set at 5×10^5 and 10^4 for the survey and MS/MS scans, respectively. MS survey scan in the Orbitrap was acquired in one microscan. Fragment ion spectra were acquired in the LTQ as an average of three microscans. Mass spectrometry data processing, data searching against TAIR10 using Mascot, and subsequent filtering and quantification based on normalized and adjusted spectral counts was performed as described (Friso et al., 2011) and as outlined in Supplemental Figure 5. Mass spectrometry-derived information and annotation of protein name, location, and function for the identified proteins can be found in the Plant Proteome Database (http://ppdb.tc.cornell.edu/). The 66 RAW MS files (Thermo), peak lists (MGF files), and search results (as Pride XML files) are available through ProteomeXchange (http://www.proteomexchange.org/).

Significance Analysis of Large-Scale Spectral Counting-Based Quantification

The GLEE software was developed using Python (with packages such as Numpy, SciPy, and Matplotlib), and a standalone executable version of the software was created using the PyInstaller program (A. Poliakov, L. Ponnala, P.D. Olinares, and K.J. van Wijk, unpublished data). GLEE was run in a Windows platform with a cubic polynomial equation fitting and 10,000 iterations for estimation of variation. QSpec analysis was performed in LINUX platform using the QPROT software provided by Choi et al. (2008). Markov chain Monte Carlo simulations were performed with a burn-in period of 5000 and 20,000 iterations to ensure convergence of the algorithm. No normalization by protein length or peptide length was included.

Assignment of Functional Categories

Protein functions were assigned using the MapMan bin system (Thimm et al., 2004) that we further curated and incorporated into the Plant Proteome Database at http://ppdb.tc.cornell.edu.

Accession Numbers

Sequence data from this article can be found in the Arabidopsis Genome Initiative under the following accession numbers: AT5G50920, ClpC1; AT3G48870, ClpC2; ATCG00670 ClpP1; AT1G66670, ClpP3; AT5G45390, ClpP4; AT1G02560, ClpP5; AT1G11750, ClpP6; AT1G49970, ClpR1; AT1G12410, ClpR2; AT1G09130, ClpR3; AT4G17040, ClpR4; AT4G25370, ClpT1; AT4G12060, ClpT2; and AT5G20720, CPN20.

Supplemental Data

Supplemental Figure 1. Primary Arabidopsis ClpT1 and ClpT2 sequences, their alignment, and mass spectrometry-based identification.

Supplemental Figure 2. Sequence conservation of ClpT1 and ClpT2 homologs in higher plants illustrated by sequence logos.

Supplemental Figure 3. Analysis of *CLPT1* transcript accumulation in the wild type and *clpt1-2*.

Supplemental Figure 4. ClpT single and double mutant phenotypes, complementations with StrepII-tagged transgenes, and comparison of the growth phenotype to *clpr2-1*.

Supplemental Figure 5. Comparative proteome analysis of wild-type and *clpt1-2 clpt2-1* seedlings grown on soil.

Supplemental Figure 6. Structural conservation of the glutamate binding pocket in ClpT1, CLPT2, and N-domains of bacterial ClpA/C chaperones.

Supplemental Figure 7. Probing the in vivo significance of the glutamate binding pocket domain through complementation.

Supplemental Figure 8. Probing the in vivo significance of the MYFF domain through complementation.

Supplemental Table 1. Determination of the approximate molar ratio between ClpT proteins and the ClpPR core in total Arabidopsis leaf extracts based on label-free mass spectrometry and spectral counting.

Supplemental Table 2. Primers used in this article.

Supplemental Table 3. Identification and quantification of proteins interacting in vivo with StrepII-tagged version of ClpT1 or ClpT2 expressed in the *clpt1-2 clpt2-1* mutant.

Supplemental Data Set 1. Fifty ClpT plant and two moss protein sequences with their accession numbers from Phytozome used for the phylogenetic analysis (cladogram) in Figure 1A.

Supplemental Data Set 2. Sequence alignments (after removal of gaps) used for generation of the cladogram in Figure 1A.

Supplemental Data Set 3. Large-scale comparative proteomics of the wild type and the *clpt1-2 clpt2-1* double homozygous mutant.

ACKNOWLEDGMENTS

M.S.K. thanks P. Grochulski and S. Labiuk at Canadian Light Source for help in synchrotron data collection. This research was supported by a grant from the National Science Foundation (MCB1021963) to K.J.V.W. and by a Discovery Grant from the National Science and Engineering Research Council of Canada (327280) to M.S.K.

AUTHOR CONTRIBUTIONS

J.K., M.S.K., K.N., G.F., and L.S. designed and performed the experimental analysis. L.P. carried out the statistical and correlation analyses. G.F. carried out all mass spectrometry analyses. M.S.K. and L.S. carried out the structural analysis. K.J.V.W., J.K., and M.S.K. wrote the article. K.J.V.W. obtained the funding for this project, recruited the coauthors, and provided general oversight.

Received February 4, 2015; revised March 19, 2015; accepted April 8, 2015; published April 28, 2015.

REFERENCES

Adams, P.D., Grosse-Kunstleve, R.W., Hung, L.W., Ioerger, T.R., McCoy, A.J., Moriarty, N.W., Read, R.J., Sacchettini, J.C., Sauter, N.K., and Terwilliger, T.C. (2002). PHENIX: building new software for automated crystallographic structure determination. Acta Crystallogr. D Biol. Crystallogr. **58:** 1948–1954.

Alexopoulos, J.A., Guarné, A., and Ortega, J. (2012). ClpP: a structurally dynamic protease regulated by AAA+ proteins. J. Struct. Biol. **179:** 202–210.

Baier, A., Winkler, W., Korte, T., Lockau, W., and Karradt, A. (2014). Degradation of phycobilisomes in Synechocystis sp. PCC6803: evidence for essential formation of an NblA1/NblA2 heterodimer and its codegradation by A Clp protease complex. J. Biol. Chem. **289:** 11755–11766.

Choi, H., Fermin, D., and Nesvizhskii, A.I. (2008). Significance analysis of spectral count data in label-free shotgun proteomics. Mol. Cell. Proteomics **7:** 2373–2385.

Colombo, C.V., Ceccarelli, E.A., and Rosano, G.L. (2014). Characterization of the accessory protein ClpT1 from *Arabidopsis thaliana*: oligomerization status and interaction with Hsp100 chaperones. BMC Plant Biol. **14:** 228.

Curtis, M.D., and Grossniklaus, U. (2003). A Gateway cloning vector set for high-throughput functional analysis of genes in planta. Plant Physiol. **133:** 462–469.

Derrien, B., Majeran, W., Effantin, G., Ebenezer, J., Friso, G., van Wijk, K.J., Steven, A.C., Maurizi, M.R., and Vallon, O. (2012). The purification of the *Chlamydomonas reinhardtii* chloroplast ClpP complex: additional subunits and structural features. Plant Mol. Biol. **80:** 189–202.

Emsley, P., and Cowtan, K. (2004). Coot: model-building tools for molecular graphics. Acta Crystallogr. D Biol. Crystallogr. **60:** 2126–2132.

Erbse, A.H., Wagner, J.N., Truscott, K.N., Spall, S.K., Kirstein, J., Zeth, K., Turgay, K., Mogk, A., Bukau, B., and Dougan, D.A. (2008). Conserved residues in the N-domain of the AAA+ chaperone ClpA regulate substrate recognition and unfolding. FEBS J. **275:** 1400–1410.

Forsberg, J., Ström, J., Kieselbach, T., Larsson, H., Alexciev, K., Engström, Å., and Åkerlund, H.-E. (2005). Protease activities in the chloroplast capable of cleaving an LHCII N-terminal peptide. Physiol. Plant. **123:** 21–29.

Friso, G., Olinares, P.D.B., and van Wijk, K.J. (2011). The workflow for quantitative proteome analysis of chloroplast development and differentiation, chloroplast mutants, and potein interactions by spectral counting. In Chloroplast Research in Arabidopsis, R.P. Jarvis, ed (New York: Humana Press), pp. 265–282.

Guo, F., Esser, L., Singh, S.K., Maurizi, M.R., and Xia, D. (2002). Crystal structure of the heterodimeric complex of the adaptor, ClpS, with the N-domain of the AAA+ chaperone, ClpA. J. Biol. Chem. **277:** 46753–46762.

Huang, M., Friso, G., Nishimura, K., Qu, X., Olinares, P.D., Majeran, W., Sun, Q., and van Wijk, K.J. (2013). Construction of plastid reference proteomes for maize and Arabidopsis and evaluation of their orthologous relationships; the concept of orthoproteomics. J. Proteome Res. **12:** 491–504.

Kabsch, W. (2010). Xds. Acta Crystallogr. D Biol. Crystallogr. **66:** 125–132.

Karradt, A., Sobanski, J., Mattow, J., Lockau, W., and Baier, K. (2008). NblA, a key protein of phycobilisome degradation, interacts with ClpC, a HSP100 chaperone partner of a cyanobacterial Clp protease. J. Biol. Chem. **283:** 32394–32403.

Kato, Y., and Sakamoto, W. (2010). New insights into the types and function of proteases in plastids. Int. Rev. Cell Mol. Biol. **280:** 185–218.

Kim, J., Olinares, P.D., Oh, S.H., Ghisaura, S., Poliakov, A., Ponnala, L., and van Wijk, K.J. (2013). Modified Clp protease complex in the ClpP3 null mutant and consequences for chloroplast development and function in Arabidopsis. Plant Physiol. **162:** 157–179.

Kim, J., Rudella, A., Ramirez Rodriguez, V., Zybailov, B., Olinares, P.D., and van Wijk, K.J. (2009). Subunits of the plastid ClpPR protease complex have differential contributions to embryogenesis, plastid biogenesis, and plant development in Arabidopsis. Plant Cell **21:** 1669–1692.

Kim, Y.I., Levchenko, I., Fraczkowska, K., Woodruff, R.V., Sauer, R.T., and Baker, T.A. (2001). Molecular determinants of complex formation between Clp/Hsp100 ATPases and the ClpP peptidase. Nat. Struct. Biol. **8:** 230–233.

Kirstein, J., Molière, N., Dougan, D.A., and Turgay, K. (2009). Adapting the machine: adaptor proteins for Hsp100/Clp and AAA+ proteases. Nat. Rev. Microbiol. **7:** 589–599.

Kmiec, B., Teixeira, P.F., and Glaser, E. (2014). Phenotypical consequences of expressing the dually targeted presequence protease, AtPreP, exclusively in mitochondria. Biochimie **100:** 167–170.

Kmiec, B., et al. (2013). Organellar oligopeptidase (OOP) provides a complementary pathway for targeting peptide degradation in mitochondria and chloroplasts. Proc. Natl. Acad. Sci. USA **110:** E3761–E3769.

Koumoto, Y., Shimada, T., Kondo, M., Takao, T., Shimonishi, Y., Hara-Nishimura, I., and Nishimura, M. (1999). Chloroplast Cpn20 forms a tetrameric structure in *Arabidopsis thaliana*. Plant J. **17:** 467–477.

Kress, W., Maglica, Z., and Weber-Ban, E. (2009). Clp chaperone-proteases: structure and function. Res. Microbiol. **160:** 618–628.

Liu, K., Ologbenla, A., and Houry, W.A. (2014). Dynamics of the ClpP serine protease: a model for self-compartmentalized proteases. Crit. Rev. Biochem. Mol. Biol. **49:** 400–412.

Lukowitz, W., Gillmor, C.S., and Scheible, W.R. (2000). Positional cloning in Arabidopsis. Why it feels good to have a genome initiative working for you. Plant Physiol. **123:** 795–805.

Lundquist, P.K., Poliakov, A., Bhuiyan, N.H., Zybailov, B., Sun, Q., and van Wijk, K.J. (2012). The functional network of the Arabidopsis plastoglobule proteome based on quantitative proteomics and genome-wide coexpression analysis. Plant Physiol. **158:** 1172–1192.

Maglica, Z., Kolygo, K., and Weber-Ban, E. (2009). Optimal efficiency of ClpAP and ClpXP chaperone-proteases is achieved by architectural symmetry. Structure **17:** 508–516.

McCoy, A.J., Grosse-Kunstleve, R.W., Adams, P.D., Winn, M.D., Storoni, L.C., and Read, R.J. (2007). Phaser crystallographic software. J. Appl. Cryst. **40:** 658–674.

Nishimura, K., and van Wijk, K.J. (2014). Organization, function and substrates of the essential Clp protease system in plastids. Biochim. Biophys. Acta **pii:** S0005–S2728.

Nishimura, K., Asakura, Y., Friso, G., Kim, J., Oh, S.H., Rutschow, H., Ponnala, L., and van Wijk, K.J. (2013). ClpS1 is a conserved substrate selector for the chloroplast Clp protease system in Arabidopsis. Plant Cell **25:** 2276–2301.

Olinares, P.D., Kim, J., and van Wijk, K.J. (2011a). The Clp protease system; a central component of the chloroplast protease network. Biochim. Biophys. Acta **1807:** 999–1011.

Olinares, P.D., Kim, J., Davis, J.I., and van Wijk, K.J. (2011b). Subunit stoichiometry, evolution, and functional implications of an asymmetric plant plastid ClpP/R protease complex in Arabidopsis. Plant Cell **23:** 2348–2361.

Peltier, J.B., Ytterberg, J., Liberles, D.A., Roepstorff, P., and van Wijk, K.J. (2001). Identification of a 350-kDa ClpP protease complex with 10 different Clp isoforms in chloroplasts of *Arabidopsis thaliana*. J. Biol. Chem. **276:** 16318–16327.

Peltier, J.B., Ripoll, D.R., Friso, G., Rudella, A., Cai, Y., Ytterberg, J., Giacomelli, L., Pillardy, J., and van Wijk, K.J. (2004). Clp protease complexes from photosynthetic and non-photosynthetic plastids and mitochondria of plants, their predicted three-dimensional structures, and functional implications. J. Biol. Chem. **279:** 4768–4781.

Peltier, J.B., Cai, Y., Sun, Q., Zabrouskov, V., Giacomelli, L., Rudella, A., Ytterberg, A.J., Rutschow, H., and van Wijk, K.J. (2006). The oligomeric stromal proteome of *Arabidopsis thaliana* chloroplasts. Mol. Cell. Proteomics **5:** 114–133.

Pietrosiuk, A., Lenherr, E.D., Falk, S., Bönemann, G., Kopp, J., Zentgraf, H., Sinning, I., and Mogk, A. (2011). Molecular basis for the unique role of the AAA+ chaperone ClpV in type VI protein secretion. J. Biol. Chem. **286:** 30010–30021.

Rudella, A., Friso, G., Alonso, J.M., Ecker, J.R., and van Wijk, K.J. (2006). Downregulation of ClpR2 leads to reduced accumulation of the ClpPRS protease complex and defects in chloroplast biogenesis in Arabidopsis. Plant Cell **18:** 1704–1721.

Sauer, R.T., and Baker, T.A. (2011). AAA+ proteases: ATP-fueled machines of protein destruction. Annu. Rev. Biochem. **80:** 587–612.

Schmidt, T.G., and Skerra, A. (2007). The Strep-tag system for one-step purification and high-affinity detection or capturing of proteins. Nat. Protoc. **2:** 1528–1535.

Schuhmann, H., and Adamska, I. (2012). Deg proteases and their role in protein quality control and processing in different subcellular compartments of the plant cell. Physiol. Plant. **145:** 224–234.

Sharkia, R., Bonshtien, A.L., Mizrahi, I., Weiss, C., Niv, A., Lustig, A., Viitanen, P.V., and Azem, A. (2003). On the oligomeric state of chloroplast chaperonin 10 and chaperonin 20. Biochim. Biophys. Acta **1651:** 76–84.

Shevchenko, A., Tomas, H., Havlis, J., Olsen, J.V., and Mann, M. (2006). In-gel digestion for mass spectrometric characterization of proteins and proteomes. Nat. Protoc. **1:** 2856–2860.

Sjögren, L.L., and Clarke, A.K. (2011). Assembly of the chloroplast ATP-dependent Clp protease in Arabidopsis is regulated by the ClpT accessory proteins. Plant Cell **23:** 322–332.

Stanne, T.M., Pojidaeva, E., Andersson, F.I., and Clarke, A.K. (2007). Distinctive types of ATP-dependent Clp proteases in cyanobacteria. J. Biol. Chem. **282:** 14394–14402.

Striebel, F., Kress, W., and Weber-Ban, E. (2009). Controlled destruction: AAA+ ATPases in protein degradation from bacteria to eukaryotes. Curr. Opin. Struct. Biol. **19:** 209–217.

Teixeira, P.F., and Glaser, E. (2013). Processing peptidases in mitochondria and chloroplasts. Biochim. Biophys. Acta **1833:** 360–370.

Thimm, O., Blasing, O., Gibon, Y., Nagel, A., Meyer, S., Kruger, P., Selbig, J., Muller, L.A., Rhee, S.Y., and Stitt, M. (2004). MapMan: a user-driven tool to display genomics data sets onto diagrams of metabolic pathways and other biological processes. Plant J. **37:** 914–939.

van Wijk, K.J. (January 12, 2015). Protein maturation and proteolysis in plant plastids, mitochondria and peroxisomes. Ann. Rev. Plant Biol., in press.

Vasudevan, D., Rao, S.P., and Noble, C.G. (2013). Structural basis of mycobacterial inhibition by cyclomarin A. J. Biol. Chem. **288:** 30883–30891.

Vitlin Gruber, A., Nisemblat, S., Azem, A., and Weiss, C. (2013). The complexity of chloroplast chaperonins. Trends Plant Sci. **18:** 688–694.

Wang, F., Mei, Z., Qi, Y., Yan, C., Hu, Q., Wang, J., and Shi, Y. (2011). Structure and mechanism of the hexameric MecA-ClpC molecular machine. Nature **471:** 331–335.

Xia, D., Esser, L., Singh, S.K., Guo, F., and Maurizi, M.R. (2004). Crystallographic investigation of peptide binding sites in the N-domain of the ClpA chaperone. J. Struct. Biol. **146:** 166–179.

Yu, A.Y., and Houry, W.A. (2007). ClpP: a distinctive family of cylindrical energy-dependent serine proteases. FEBS Lett. **581:** 3749–3757.

Zeth, K., Ravelli, R.B., Paal, K., Cusack, S., Bukau, B., and Dougan, D.A. (2002). Structural analysis of the adaptor protein ClpS in complex with the N-terminal domain of ClpA. Nat. Struct. Biol. **9:** 906–911.

Zybailov, B., Rutschow, H., Friso, G., Rudella, A., Emanuelsson, O., Sun, Q., and van Wijk, K.J. (2008). Sorting signals, N-terminal modifications and abundance of the chloroplast proteome. PLoS One **3:** e1994.

Zybailov, B., Friso, G., Kim, J., Rudella, A., Rodríguez, V.R., Asakura, Y., Sun, Q., and van Wijk, K.J. (2009). Large scale comparative proteomics of a chloroplast Clp protease mutant reveals folding stress, altered protein homeostasis, and feedback regulation of metabolism. Mol. Cell. Proteomics **8:** 1789–1810.